FRACTURE CHARACTERIZATION OF CORTICAL BONE AT THE MICROMETER AND NANOMETER LENGTH SCALES

BY

OKEOGHENE O. ORIEKA

THESIS

Submitted in partial fulfillment of the requirements
for the degree of Master of Science in Civil Engineering
in the Graduate College of the
University of Illinois at Urbana-Champaign, 2016

Urbana, Illinois

Adviser:

Professor Ange-Therese Akono

ABSTRACT

Fracture in bone is common in a wide variety of health situations, and is of particular interest to structural engineers due to the adaptability of bone tissue in response to applied stresses. Investigations into the fracture processes within bone tissue can aid in developing medical therapies to combat bone fracture. Information from researching bone fracture can also aid in designing composite materials which exhibit bone's characteristic high toughness and strength. Biological materials like bone exhibit behavior and functions that are the direct product of the interactions between the hierarchical structures that form the building blocks within the material. To fully understand the mechanical properties associated with bone and relate these properties to the scale of the mechanical characterization test, mechanical testing must be designed to engage the different responses of the hierarchical structures within bone. The purpose of the research presented in this thesis is to characterize fracture in cortical bone tissue using novel methods of small-scale mechanical testing such as micro-scratch tests and nanoindentation. Specimens are chosen and prepared in a manner that facilitates reproducible testing, and rigorous experimental protocols in nanoindentation and scratch testing are applied. The presented research confirms fracture behavior through scanning electron microscopy, and then applies nonlinear fracture mechanics to determine the fracture toughness of the bone tissue. The results from this research are key findings in confirming our methods with the literature with respect to nanoindentation, and to expanding the application of the novel scratch test in fracture investigations of a complex material.

ACKNOWLEDGEMENTS

I would like to thank the civil engineering department at the University of Illinois for supporting my graduate studies by assisting me with a fellowship. I would also like to thank my advisor Dr. Ange-Therese Akono. I appreciate your immensely helpful guidance during my time at the Sustainability Under the Nanoscope Lab, and I am forever grateful.

Thanks are due to my lab mates, and especially to my office mate Caroline Johnson for her support and friendship. Thank you to Amrita Kataruka and Kavya Mendu for contributing to the analysis and experimentation reflected in this thesis. Finally, I would like to thank my parents and siblings, who are always a call away and whose support is invaluable.

TABLE OF CONTENTS

CHAPTER 1 INTRODUCTION

1.1 Industrial Context

Fracture in bone is common in a variety of situations, including sports, old age, and as a result of a myriad of bone-related diseases. Learning about the mechanical properties of bone tissue and the behavior of the material in response to the impact of fracture processes has a variety of applications in the practice of medicine.

Advances in medical science and health care practices have increased the lifespan of the average person in the United States and around the world [109]. As humans get older, their bones tend to be more fragile [148], and large impacts can lead to serious bone fractures [126, 163, 2]. Bone quality, measured in bone mineral density, degrades due to aging processes [126]. Furthermore, aging humans have to contend with a variety of bone and joint diseases, ranging from osteoporosis or the loss of strength in bone, to osteoarthritis or the breakdown of bone tissue. In fact, osteoporosis causes more than 8.9 million fractures annually, or a fracture in every 3 seconds [72] and is estimated to affect 200 million women worldwide [73], with one in two women and one in four men over the age of 50 being susceptible to an osteoporotic fracture in their lifetime [126, 128]. The economic impact of bone fracture is enormous; as much as 20.3 billion dollars has been spent in the span of a single year on medical costs aimed at treating bone fractures due to osteoporosis [27]. The investigation of bone's mechanical properties is essential to the understanding and treatment of osteoporosis and osteoarthrosis, as well as in the development of therapies used in bone fracture treatment [82]. By investigating and pinpointing the situations during which fracture occurs within bone, medical practitioners can indicate more specific diagnoses and treatments that could lead to bone fracture prevention, and the economic burden of treating diseases like osteoporosis can be alleviated.

Investigations into the fracture processes within bone can aid in developing composite materials which exhibit a high toughness and strength for a variety of uses. Bone, a material made of hierarchical structures, demonstrates nature's ability to craft a complex and functional load-bearing system that can self-repair[126, 2] in response to mechanical phenomena through years of evolution and adaptation. Due to the composite nature of bone, the material is well suited to serve several structural-mechanical functions within the body of an organism. The material balances the relationship between structure and function; bone is the direct product of a natural process to address extremely difficult structural-mechanical problems [155]. Therefore, bone presents a detailed map of the nuances between structural utility and function, and can be used by engineers and scientists to create new composites which exhibit the mechanical properties observed in the complex material [95, 154].

1.2 Research Objectives and Approach

The objective of this research is to characterize multiscale fracture processes within bone tissue through novel, sustainable, and small-scale mechanical testing and analysis methods. The focus on developing a small-scale testing regime is integral to the presented research because of the composition of bone; the material's characteristics are dependent on its hierarchical structure and the interactions of different components at multiple scales of observation.

One of the most important mechanical properties of bone is the inherent ability to resist fracture through toughening mechanisms. Bone is a low-density structural material that exhibits desirable characteristics such as high stiffness, high strength and high fracture toughness [45, 43]. The high fracture toughness found in bone is coupled with a low elastic or Young's modulus [158], which is defined as the rela-

tionship between the applied stress and the resultant strain. The fracture toughness, defined in magnitude by the critical stress intensity factor, K_c, is a measure of the resistance to brittle fracture in the presence of a crack, and is dependent on the elastic modulus and toughness [158, 97]. Therefore, the main objective of the research is to conduct an in-depth investigation of fracture processes within bone, to quantify bone's fracture toughness and related properties through mechanical testing, and to compare the results with previously published approaches.

The fracture toughness of bone can be explained by considering two sources of toughness; the intrinsic toughening mechanisms which create ductility and plasticity within the tissue of the bone and promote cracking, and the extrinsic toughening mechanisms which keep large cracks from growing under increasing stresses or strains [163, 2, 162]. These toughening mechanisms should be observable during and after mechanical testing, to confirm that fracture processes are in fact induced by our test, the scratch test.

The bulk fracture toughness and other mechanical properties of bone have been investigated by a myriad of large-scale mechanical tests. However, large-scale testing requires a large amount of specimens, and does not accurately represent the microscale properties inherent in a hierarchical material like bone. An important aspect of investigating a hierarchical and complex material like bone is an in-depth consideration of the scale at which fracture is induced during mechanical testing, therefore, a number of different techniques must be combined to discern more about the characteristics of each length scale [96, 119]. Newly developed nano-scale and micro-scale mechanical testing techniques, like scratch testing and nanoindentation, are necessary to efficiently gather data while conserving bone tissue material. For material analysis, optical microscopy, x-ray diffraction, and scanning electron microscopy are methods which have been used to obtain structural information at such a small scale [119].

These methods are fundamental in observing the fracture phenomena exhibited by the material.

Because mechanical testing is currently not advanced enough to characterize the mechanical properties of bone tissue in living organisms, other specimen sources and testing methods have to be considered to simulate in-vivo properties. The presented research focuses on investigating the mechanical properties of carefully prepared porcine and bovine cortical bone specimens. Most investigations on the mechanical properties of bone tissue are done on specimens extracted from cadavers, with the assumption that the in-vivo properties will be adequately represented by the cadaveric bone properties [82]. The porcine species were specifically chosen because pigs have a comparable physiology and anatomy to humans, and are recognized as an adequate model of human tissue behavior [45]. The bovine specimens were chosen to refine the developed preparation and testing procedures on specimens with a larger consistent area.

1.3 Thesis Outline

The first part of this thesis provides an introduction to the general research. Chapter 1 presents the industrial context under which the presented research is carried out, and discusses the objectives for this particular study, as well as the methods used to approach the investigation. Chapter 1 also provides an insight into the significance of the presented research on the process of characterizing bone fracture. Chapter 2 presents a foundation for understanding the composition of bone tissue and the structural-mechanical properties of the hierarchical components within the material.

The second part of this thesis presents the method for creating specimens. Chapter 3 details the source of the specimens, as well as the important laboratory equipment

used in creating a sample. Chapter 4 describes the sample preparation and storage procedures, and includes an account of previously tried preparation protocols as well as the challenges faced in developing a working procedure.

The third part of this thesis describes the theory and methodology of the mechanical testing procedures utilized in this study. Chapter 5 and Chapter 6 focus on nanoindentation and scratch testing respectively, and presents the background theory behind each test, how each test is applied in the study, and the analysis procedures utilized in interpreting the resultant data.

The fourth part of the thesis summarizes the results from mechanical testing and details the conclusions drawn from the performed research and the accompanying perspectives for future work.

1.4 Research Significance

Investigating the structural-mechanical properties of bone has been the subject of several papers and journal entries, and a variety of mechanical tests have been utilized during experimentation. However, most methods used in the determination of the mechanical properties in bone only capture a single mode of fracture in the bulk material. This approach does not accurately portray the influence of the hierarchical structural makeup of bone.

The significance of this study lies in the methods used to characterize the mixed-mode fracture properties of the material. The presented research focuses on a novel and sustainable approach to testing the material by avoiding the use of harsh chemicals in the sample preparation procedure, and using small-scale mechanical tests for a more accurate characterization of the material's hierarchical structure. These small scale tests include nanoindentation, which yields the hardness value and the elastic

modulus, and scratch tests, which will be used in determining the fracture toughness. While the scratch test has been used in material science to investigate adhesion or wear in metallic specimens and thin coatings [26, 22, 34, 78, 92], this research aims to provide evidence of the scratch test's viability in the fracture characterization of a complex, hierarchical, and biological material such as cortical bone. Because the scratch occurs with a vertical and horizontal force component, the scratch test forces a mixed-mode fracture to occur, which activates the inherent toughening mechanisms in bone.

1.5 Chapter Summary

This chapter provides an introduction to the fracture characterization of bone by supplying an industrial context for studying fracture in bone, and explaining the research objectives and approach for this particular investigation. The chapter also delineates the outline of the thesis, and demonstrates the significance of using small-scale testing as the basis of the investigation.

CHAPTER 2 BACKGROUND

Biological materials exhibit behavior and functions that are the direct product of the interactions between the multi-scale constituent components that form the building blocks within the material [91]. This is especially true for bone tissue because of the material's hierarchical composition. To fully understand the mechanical properties associated with bone and relate these properties to the scale of the mechanical characterization test, an overview of bone as a biological material is necessary.

2.1 Histology of Bone

The macrostructure of bone is comprised of the cortical and trabecular bone, as displayed in the femoral X-ray in Figure 2.1. The microstructure is comprised of the osteons, Haversian canals, and lamellae, and the nanostructure is comprised of the collagen fibrils and the bone mineral crystals [119]. Each of these structures contributes to the structural-mechanical properties exhibited by the bone, and each structure has distinct mechanical characteristics. The combination of these structures in bone creates a heterogeneous and anisotropic material [119].

The hierarchical nature of bone represents the different structures in which the mineralized collagen fibrils are organized. The bone can be divided into two distinct parts – the compact or cortical bone which forms the outer shell, and the trabecular bone which forms the inner shell. As Figure 2.1 shows, cortical bone is denser than trabecular bone. The difference in density is due to their biological functions. Cortical bone is the key component in formulating bone's mechanical responses to applied forces by providing rigid support and protection for the organs [87]. The cortical shell also contains calcium, a necessary element for the health of most organisms [6]. The inner trabecular bone is a spongy mass which facilitates metabolic activity within

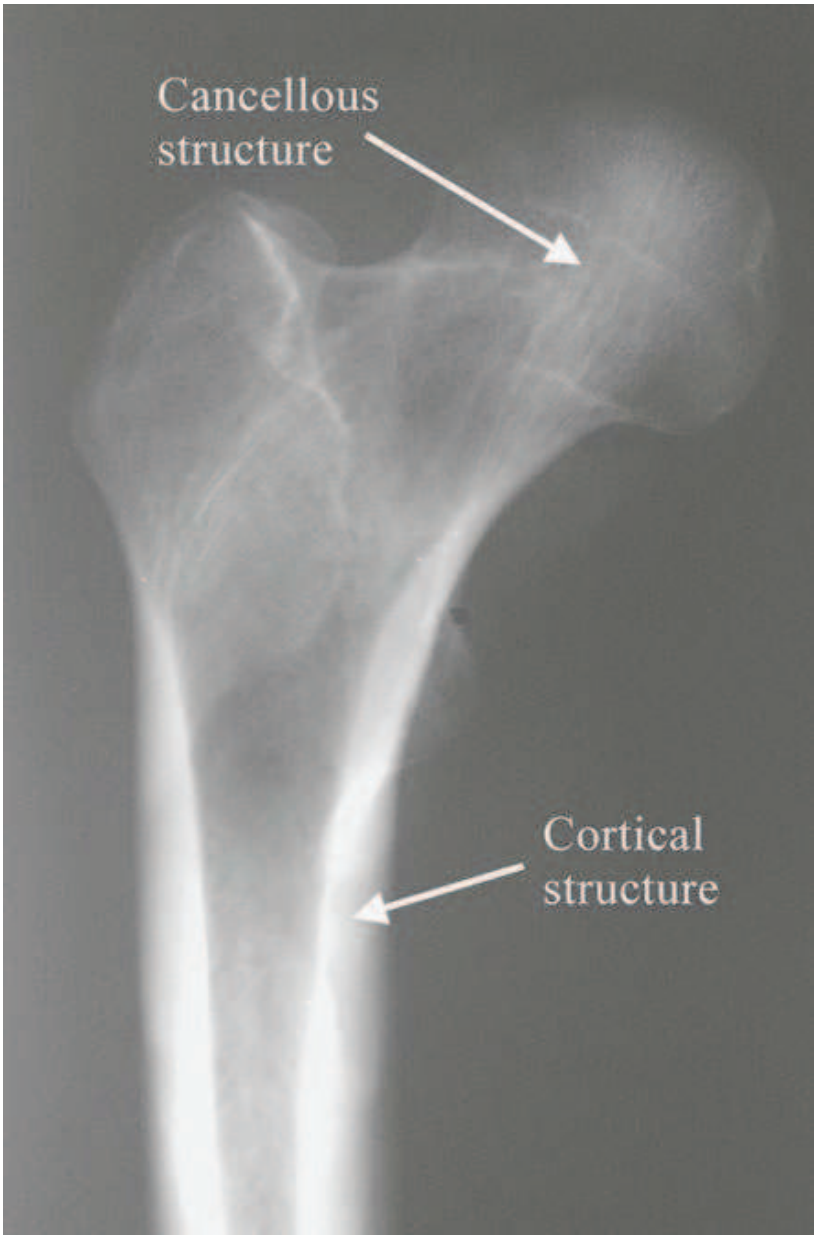

Figure 2.1: X-Ray image of femoral bone featuring the observable difference in density between the cortical bone and trabecular bone (from [6]).

the bone [6]. Trabecular bone is also important in redistributing stresses within bone, and adds to the resilience, high toughness, and high strength observed in macroscopic bone [87].

The compact bone tissue is comprised of cylindrical osteons which run longitudinally with respect to the long axis of the bone. A cross-section of bone tissue displaying the constituent structures is displayed in Figure 2.2. The cross section shows the outer circumferential lamellae and osteons which form the outermost shell of the cortical bone. The osteons develop their notable cylindrical geometry and distribution closer to the center of the bone. These osteons are formed with the mineralized collagen fibril arrays, which are arranged in several different patterns.

As bone adapts to its surroundings, the bone reconstitutes its internal matrix. The osteoclast cells create a large tunnel within the matrix, and the osteoblast cells deposit cementitious material and lamellae onto the surface of the tunnel, forming a blood vessel channel within the bone itself [155]. This channel, surrounded by layers of lamellae and mineralized fibrils, forms a single osteon or Haversian canal system. The osteon is about 200 μm to 250 μm in diameter and is typically oriented parallel to the long axis of the bone.

The mineralized collagen fibrils consist of a three-dimensional protein matrix supporting a growth of carbonated apatite crystals [155]. The carbon apatite crystals grow in the form of a thin, uniform plate, and have an average length of 50 nm, an average width of 25 nm, and a thickness range of 1.5 nm to 4.0 nm [155]. The type I collagen fibril in bone structures has a diameter of 80 nm to 100 nm, and their lengths cannot be completely determined as fibrils tend to grow into one another [155]. Mineralized collagen fibrils arrange themselves into planar lamellae sheets, which are about 3 μm to 7 μm thick [119].

Due to the intricacy of bone tissue, samples need to be characterized on a multi-

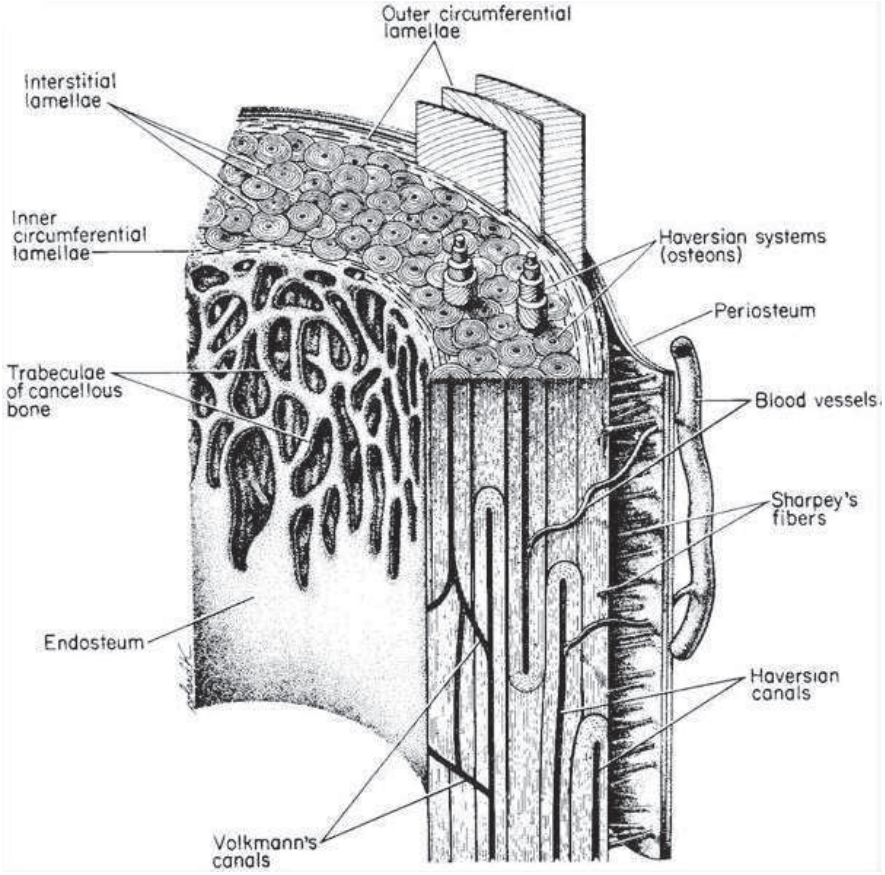

Figure 2.2: Cross-section of a bone displaying the different hierarchical structures within (from [87]).

scale level by considering the hierarchical structure of the material. The hierarchical structure is important in investigating cracks at different length scales, as the scale of the crack determines the affected structures and fracture mechanisms involved in analyzing the results [96]. Researchers throughout the years have accomplished this through a variety of methods and devices that can characterize the structures within the bone as well as the fracture processes that can be observed; these characterization methods range from the macro-scale to the nano-scale. These methods include imaging the hierarchical structures within bone with scanning electron microscopy [94, 158] and environmental scanning electron microscopy and fractography [76], coupled with image analyses [94, 158]. X-ray micro-computed tomography has been utilized to characterize the fracture surfaces in bone tissue, as well as the number and size of osteons in a particular sample area[164, 76, 36]. Fourier transform infrared spectroscopy has been used to determine the quality and integrity of the collagen matrix within bone samples by measuring mineral content [8, 46, 1], while X-ray diffraction has been used to investigate mineralization levels [16, 57, 119, 71]. Raman spectroscopy has been used to study the effects of aging on cortical bone due to its sensitive measurement of organic material within bone and a finer spatial resolution in imaging [1]. Each method has contributed to the understanding of how the different components are arranged within bone tissue, and how the histology of bone affects the material's mechanical properties on a multiscale level.

2.2 Composition of Bone

The skeletal system, shown in Figure 2.3, provides a rigid network of structural support and stability to the organs within an organism, and is made up of several building blocks commonly referred to as bone. Bones perform a variety of functions within

the body, and serve as a system of protection for some of the most vital organs in the body of an organism, including the central nervous system, and the cranial, thoracic, and pelvic viscera [40]. In addition to comprising the skeletal system's important protective functions, bone tissue also houses healing cells and contributes to mineral ion homeostasis within the body [119].

To fulfill these essential purposes of protection as well as structural support and stability, bones must be capable of withstanding gravitational forces from the weight of the organs being carried; bones must also be capable of withstanding impact forces in several orientations from a myriad of mechanical situations, such as jumping, running, or falling. Bones may handle these two broad types of forces actively by allowing some degree of movement in relation to the applied forces through elastic deformations, or passively, by resisting the forces through strength properties as a result of plastic yielding [40, 104]. The strength characteristics in bone contribute to its uniqueness because bone can resist compressive forces, as well as large impact forces or bending stresses [155].

Bone contributes to the general functioning of the body of an organism by providing support through its structural-mechanical properties, creating blood through the marrow, and acting as a storage facility for calcium and phosphorus [127]. To fully understand the relationship between the structure and function of bone, a review of the different hierarchical structural models is presented below.

Bone's strength, toughness, and fracture resistance can be further explained by an investigation of the constituent components of each hierarchical structure [163]. Bone is a composite material made of water and carbonated apatite minerals growing on a collagen matrix [8, 158, 12]. These three components contribute to the inherent material properties in bone by arranging themselves in different, higher-order structures, which can be observed at different length-scales and exhibit a variety of

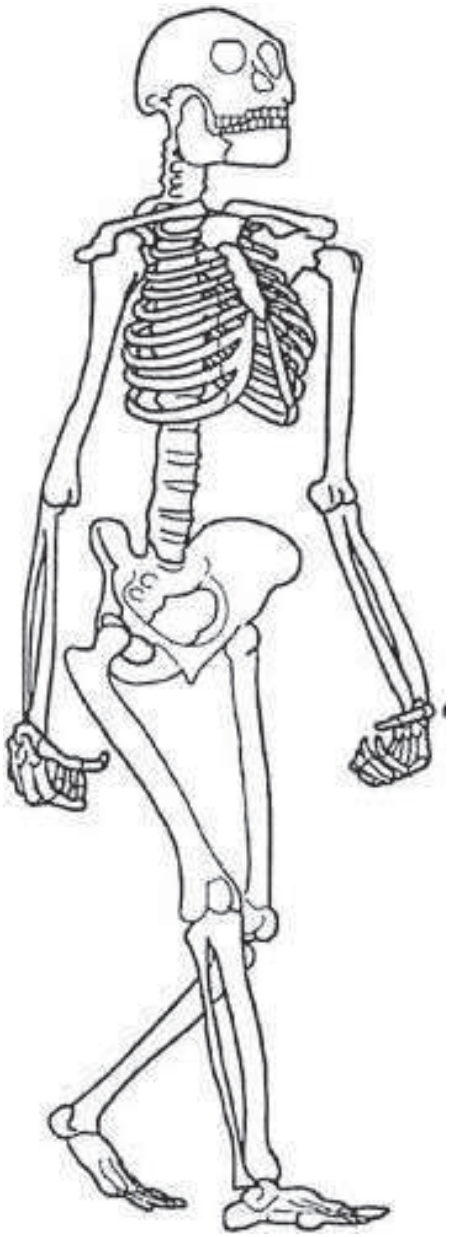

Figure 2.3: Human skeleton in motion (from [87]).

structural-mechanical properties. The complexity in this structure can be found in other materials similar to bone, including dentin, cementum, and antlers [155, 95].

A generalized model as shown in Figure 2.4 depicts bone as a material with five hierarchical levels [120, 119, 155, 104, 38]. The sub-nanostructure consists of the collagen, water, and hydroxyapatite molecules. At the nanostructural level, the basic building blocks of bone are the mineralized collagen fibrils [56]. These fibers are also composite; the constituent mineral in the fibers is called dahllite or carbonated apatite ($Ca_5(PO_4, CO_3)_3(OH)$). The carbonated apatite grows upon a three-dimensional matrix made of fibrous cross-linked protein collagen molecules and water [155, 56]. The protein matrix upon which the carbonated apatite grows is typically comprised of type I collagen [155]. The matrix of mineralized collagen contributes to the viscoelastic properties and fracture resistance of bone on the microscopic scale [119]. At the sub-microstructural level, the mineralized collagen fibrils assemble into an extrafibrillar hydroxyapatite matrix known as a lamella; the lamella features lacunar cavities within it [56, 119, 155]. At the microstructural level, the lamellae form concentric cylindrical structures known as osteons, which surround Haversian canals. The lamellae also form the interstitial matrix that cements the osteons together [56]. The neo-structural level and macrostructural levels are usually represented together [56, 38]; the neo-structural level features several osteons and Haversian canals, while the macrostructure represents the whole bone containing both cortical and trabecular bone [56].

The Hellmich model [51, 52, 59, 100, 61, 58, 60, 33] as shown in Figure 2.5 depicts bone tissue as consisting of compact and trabecular bone. At a scale of 100 μm to several mm, compact bone consists of cylindrical osteons, and trabecular bone consists of trabecular struts or plates. The building block of the osteons and trabecular struts is known as the extracellular solid bone matrix, which forms the ultrastructure

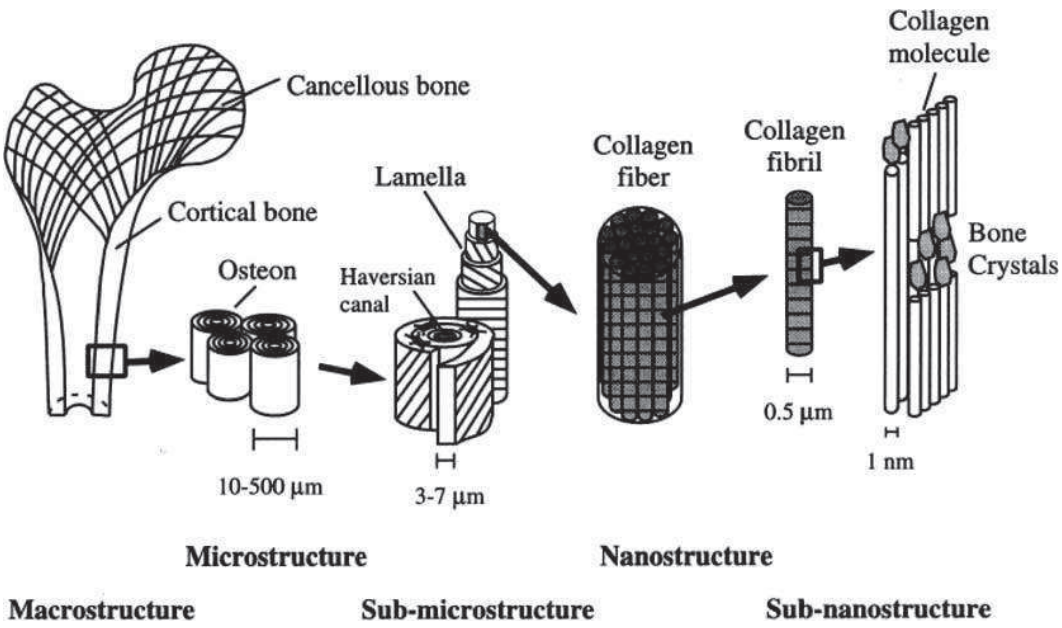

Figure 2.4: The five main hierarchical structures in bone tissue (from [104]).

of bone tissue and consists of mineralized collagen fibrils and extrafibrillar space. This scale is observable at 1 – 10 μm. At the smallest observation scale at the nanometer scale, bone tissue is made up of plate-shaped mineral crystals consisting of impure hydroxyapatite and long cylindrically-shaped collagen molecules with a length of about 300 nm and a diameter of 1.2 nm; these collagen molecules assemble themselves into fibrils. Lipids, proteins, and water molecules can also be observed.

The Ritchie model as shown in Figure 2.6 describes seven hierarchies within bone structure, with the smallest features of bone consisting of a protein phase containing tropocollagen molecules. These molecules are formed from a combination of three polypeptides assembled in a triple helix [116] and held together through hydrogen bonds between the amino acids. The tropocollagen molecules are the main constituent of the mineralized collagen fibrils, which contribute to the elasticity and energy dissipation inherent in deformation within bone material [127, 126]. This col-

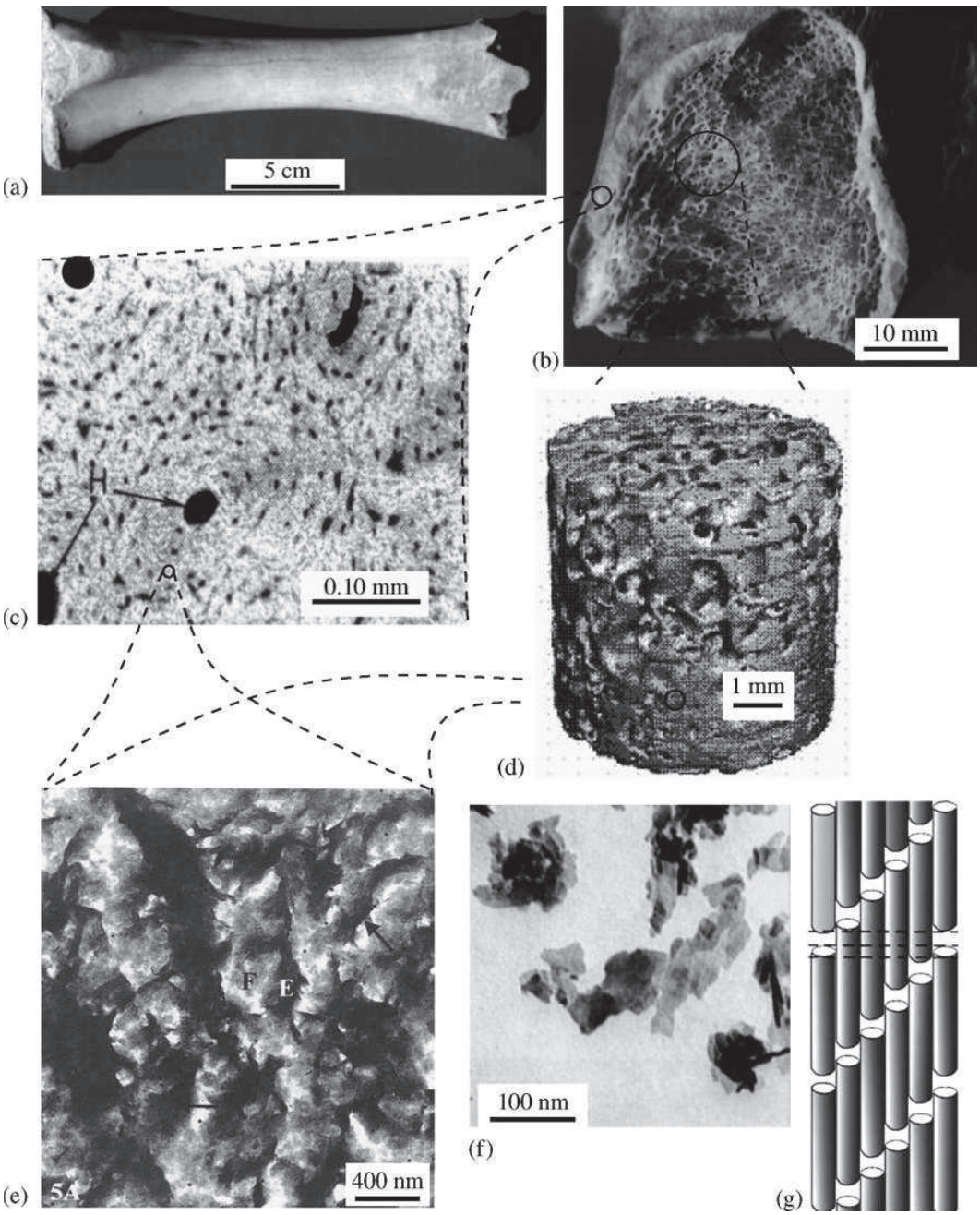

Figure 2.5: The Hellmich model of hierarchical structures of bone tissue: a) Whole long bone b) Section through long bone c) osteons in cortical bone d) trabecular spaceframe e) ultrastructure f) hydroxyapatite crystals g) collagen molecules (from [51]).

lagen consists of 90% type I collagen and 10% amorphous ground substance [126]. Collagen is also found in several other parts of the body, including cartilage, skin, and cornea [127, 126].

The collagen fibrils, with a length of 15 μm and a diameter of 50 – 70 nm [97] form arrays containing hydroxyapatite, and form the basic building block of bone tissue. These arrays are on a scale of 10 μm in length and 2 nm in width. The mineralized collagen fibril arrays arrange themselves into fibers, which arrange themselves in a patterned bundle forming lamellar structures with a thickness spanning 3-7 μm [127, 126]. The lamellar structures, or lamellae, form into osteons; osteons are cylindrical structures with diameters ranging from 200 – 300 μm. The osteons make up the Haversian system, which consists of channels within the osteons to facilitate blood flow through the bone. These osteons form the cortical bone on the macroscopic scale, which surrounds the trabecular or spongy bone [127, 126].

Developing hierarchical models is crucial to investigating the fracture response of bone; the response is always dependent on the length scale being investigated. The hierarchical nature of bone also offers an explanation for the observable bulk properties, such as high strength and toughness. These properties are attributable to the described hierarchies within each model. In the simplified model, bone's ultrastructural mechanical behavior is dependent on the mineralization process that occurs in the collagen fibrils as the hydroxyapatite molecules facilitate bonding between the collagen fibrils. The Hellmich model is based upon the same principle, and suggests that the interaction between water, collagen, and hydroxyapatite plays a leading role in facilitating the bonding and stability in the ultrastructure.

The Ritchie model builds upon previous models with the emphasis of the tropocollagen molecule's role in determining the deformation response. The investigation of the behavior of tropocollagen is crucial to appreciate the dependence of the plastic

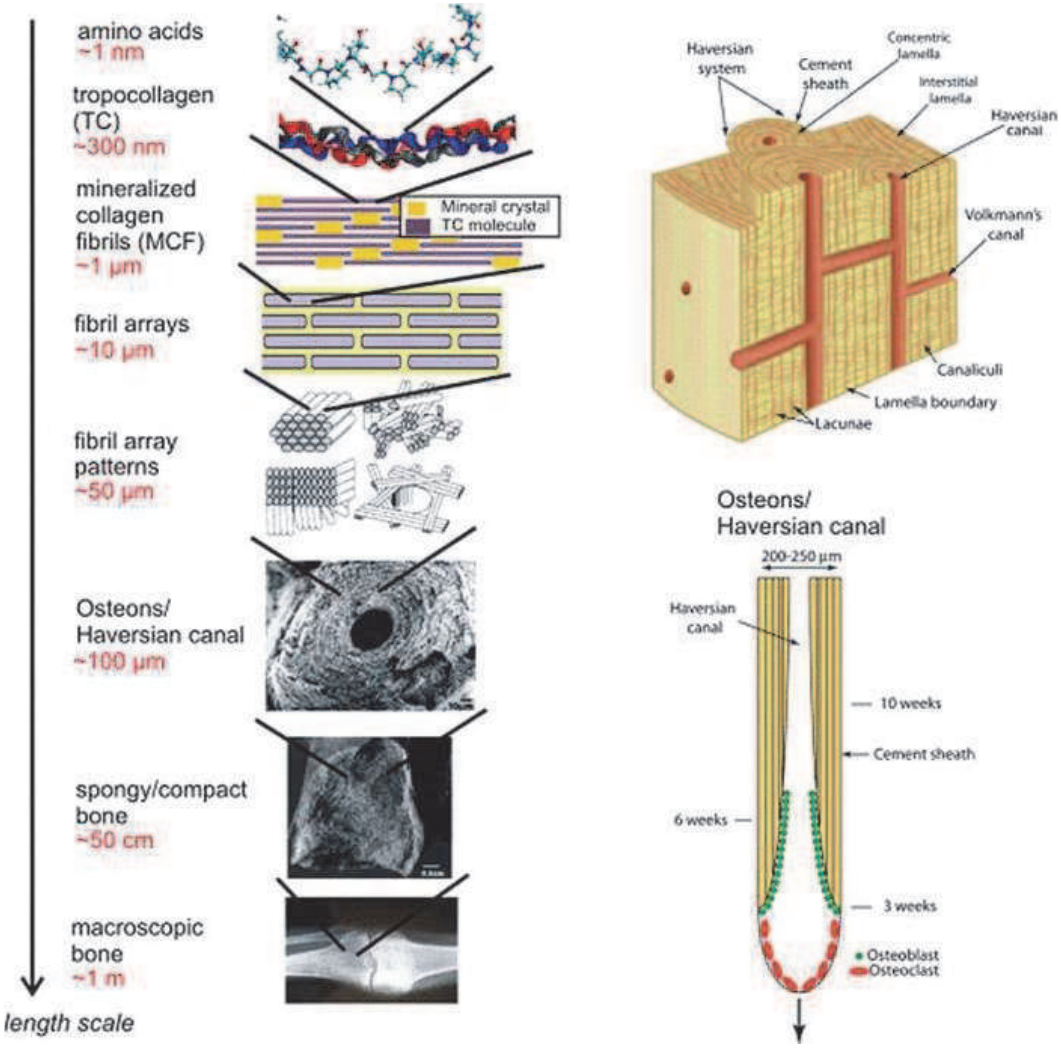

Figure 2.6: The Ritchie model of hierarchical structures within bone tissue (from [126]).

deformation within bone tissue on the hydrogen bonds within a triple helical tropocollagen molecule. As loading is applied, hydrogen bonds gradually break leading to the stretching and unwinding of individual tropocollagen molecules [127, 128]. When the strain increases, intermolecular sliding commences in the collagen fibrils leading to the breaking of strong and weak bonds between the tropocollagen molecules. The Ritchie model suggests that this intermolecular sliding is the most crucial factor in bone's ability to dissipate energy and endure large plastic strains to avoid brittle failures [127].

2.3 Mechanical Characterization at the Macroscopic Scale

While several methods have been used to determine the mechanical properties of cortical bone, previous research has indicated that cortical bone's mechanical properties are greatly influenced by porosity [131, 86], mineralization level [49, 155, 37], and the organization of the constituent solid matrix within the hierarchical structure [119, 152]. These facts mean that measured mechanical properties can vary between different regions within a bone, and from bone to bone. There is also variance in the mechanical properties due to the direction the sample is oriented in during testing, which is a result of the anisotropic nature of bone tissue. Figure 2.7 shows the standardized orientations for testing cortical bone.

The Young's modulus of cortical bone on the macroscale has been found with uniaxial tension and compression tests, as well as three-point bending tests. On the macroscopic scale, the Young's modulus of cortical bone specimens is around 10 GPa to 18 GPa [119, 117, 143, 153, 40]. A summary of research articles that present the Young's modulus of cortical bone as a result of mechanical testing performed at the macroscale is shown in Table 2.1.

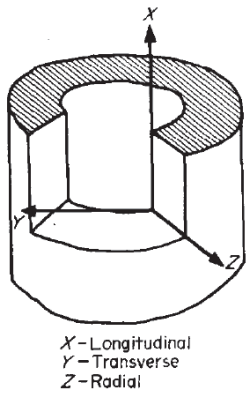

Figure 2.7: Schematic showing different orientations in cortical bone (from [117]).

Table 2.1: Summary of Young's moduli values from macroscale mechanical tests on cortical bone.

Reference	Specimen Type	Orientation of Test	Type of Test	Young's modulus in GPa
[117]	Bovine femoral bone	Transverse	Uniaxial tension and compression	12.0
[117]	Bovine femoral bone	Radial	Uniaxial tension and compression	10.0
[159]	Bovine femoral bone	Transverse	Three-point bending test	17.5
[159]	Bovine femoral bone	Longitudinal	Three-point bending test	12.1

The fracture toughness of cortical bone tissue at the macroscopic level has been verified by several research papers with a variety of mechanical tests that measure crack propagation as a result of an initial crack. These tests include single-edge notched beam tests [17, 159, 88], compact tension tests [32, 117, 29, 129], compact sandwich tests [151, 153, 150], chevron-notched three-point bending tests [158, 96, 129], and fatigued pre-cracked beam tests [158, 42].

Fracture toughness investigations on notched samples were first conducted with single-edge notch beam tests on cortical bone specimens by Melvin and Evans [89]; the tests determine a mean stress intensity factor K_c as a result of the controlled crack propagation due to bending applied to a beam-shaped sample with a notch in the center of the specimen, as shown in Figure 2.8. Notched tests have been applied to bovine femoral and tibial cortical bone specimens to induce fracture in the longitudinal and transverse directions. Figure 2.9 shows a schematic of a typical notched specimen from a bovine femur, as well as micrographs of the notches within the specimen. A summary of research articles on macroscale cortical bone investigations that present the fracture toughness as embodied by the stress intensity factor is displayed in Table 2.2.

2.4 Mechanical Characterization at the Microscopic Scale

Understanding the behavior of bone tissue and characterizing the fracture response at small scales is predicated on investigating the elastic characteristics of the response of bone tissue to applied loading [117]. For microscopic scale analyses, a major challenge consists of selecting a physics-based constitutive model for bone tissue. Several models have been proposed including linear elastic isotropic, transversely isotropic, or orthotropic, each characterized by their corresponding elastic constants [117]. The

Table 2.2: Summary of stress intensity factors K_c from macroscale tests on cortical bone.

Reference	Specimen Type	Orientation of Test	Type of Test	K_c in $MPa\sqrt{m}$
[89]	Bovine femoral bone	Longitudinal	Single-edge notch beam	3.21
[89]	Bovine femoral bone	Transverse	Single-edge notch beam	5.49
[17]	Bovine tibial bone	Transverse	Single-edge notch beam	6.56
[157]	Bovine femoral bone	Longitudinal	Compact tension test	2.39 - 4.97
[18]	Bovine femoral bone	Transverse	Single-edge notch beam	2.2 - 4.6
[129]	Bovine femoral bone	Transverse	Chevron-notched three-point bending test	3 - 8
[19]	Bovine femoral bone	Longitudinal	Compact tension test	2.4 - 5.2
[9]	Bovine femoral bone	Longitudinal	Compact tension test	4.46 - 5.38
[10]	Bovine tibial bone	Longitudinal	Compact tension test	3.2
[10]	Bovine tibial bone	Transverse	Compact tension test	6.5
[103]	Human tibial bone	Transverse	Compact tension test	3.68
[102]	Bovine tibial bone	Transverse	Compact tension test	4.93 - 12.64
[146]	Human tibial bone	Longitudinal	Compact tension test	2.25
[165]	Human femoral bone	Transverse	Compact sandwich test	6.4
[153]	Human femoral bone	Transverse	Compact sandwich test	2.25
[96]	Human humerus	Transverse	Chevron-notched three-point bending test	5.33 ± 0.41

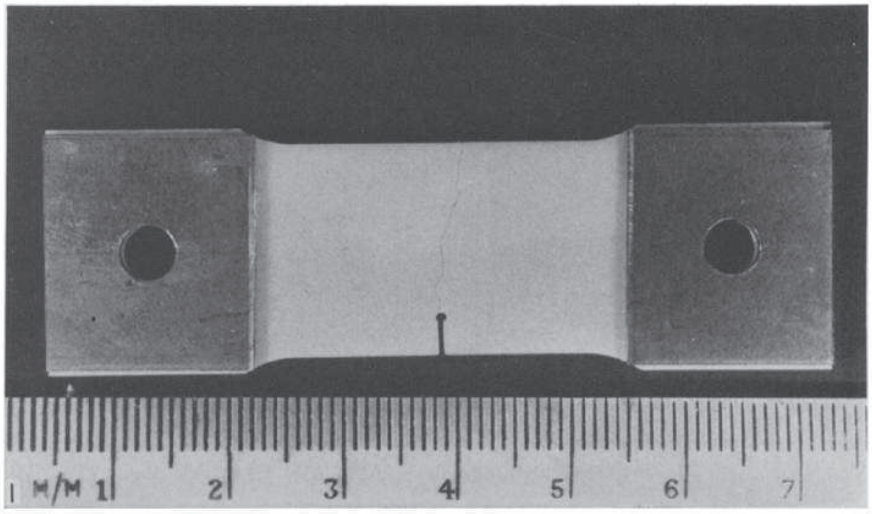

Figure 2.8: An example specimen for the single-edge notch beam test (from [18]).

linear elastic isotropic model with two elastic constants assumes that the material is homogeneous and isotropic in its constitutive behavior, which is elastic with time-independent plasticity [121, 166]. The model also assumes that all osteons are parallel with respect to each other and are all geometrically identical [77]. The transversely isotropic model considers five independent elastic constants [117] and assumes symmetry about the osteonal axis. A schematic showing the difference between the linear elastic isotropic model and the transversely isotropic model is displayed in Figure 2.10. The orthotropic model is based upon the assumption that bone tissue is an anisotropic solid, and considers nine independent elastic constants.

The Young's modulus of cortical bone tissue on the microscale level has been measured in a variety of ways; the most popular technique involves nanoindentation of a small area within the cortical bone sample. Other techniques have also been utilized, including ultrasonic testing and micro-tensile testing. A summary of the Young's moduli from published research is summarized in Table 2.3.

The fracture toughness of cortical bone on the microscale level as quantified by

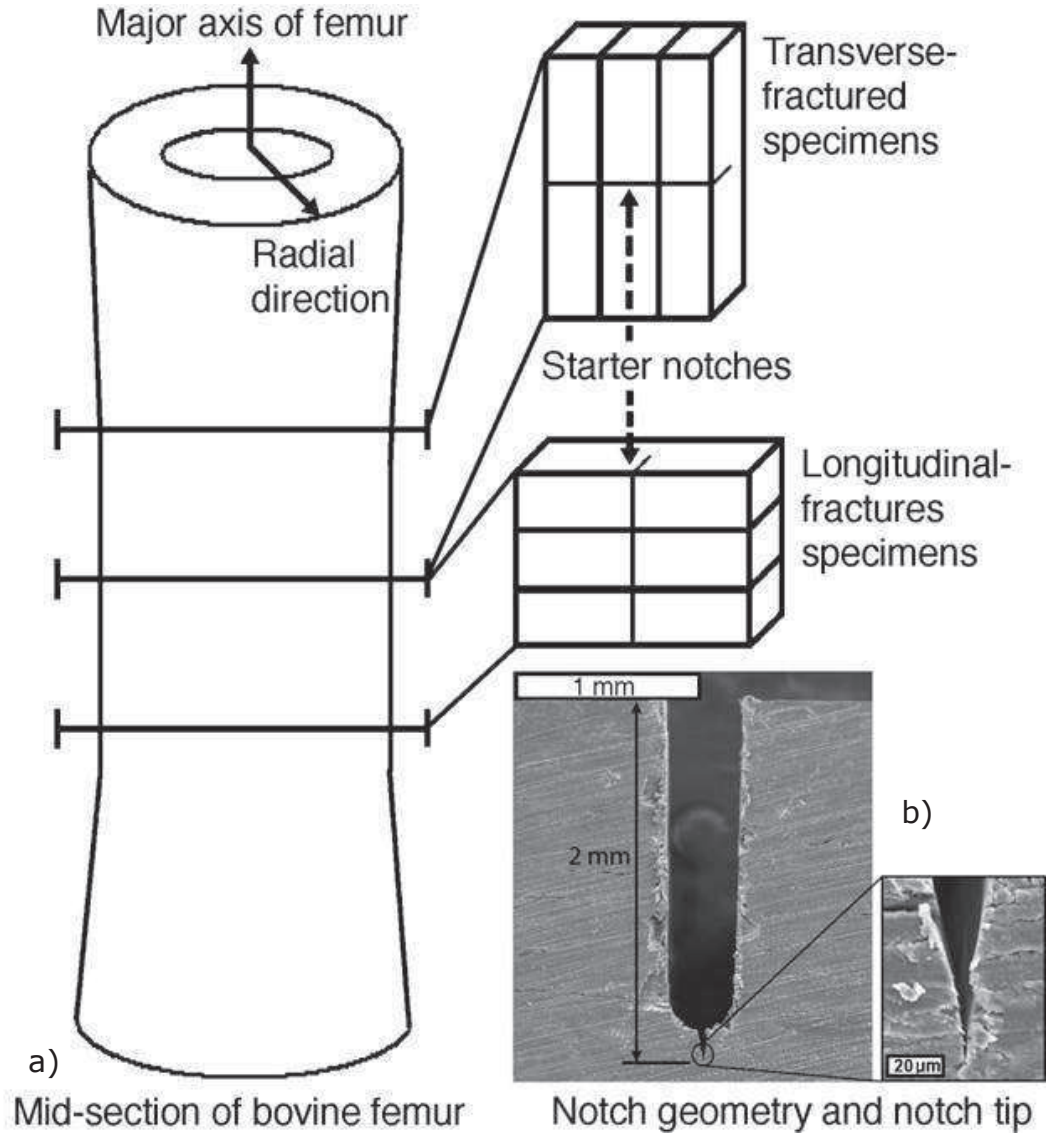

Figure 2.9: a) Schematic of potential notched specimen orientations that can be excised from the mid-section of a bovine femoral bone. b) Micrographs of a notch within cortical bone (from [159]).

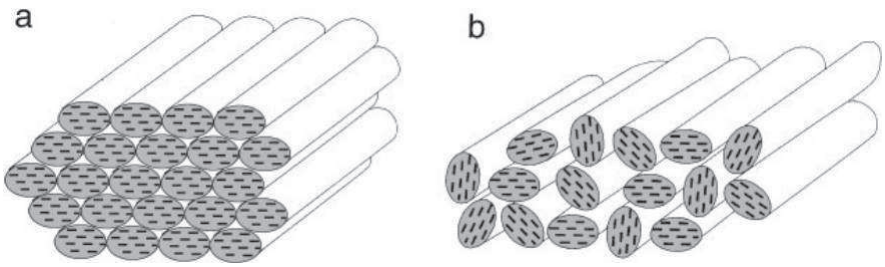

Figure 2.10: Idealization of the linear elastic isotropic model and the transversely isotroopic model. a) Linear elastic isotropic. b) Transversely isotropic. (from [155]).

Table 2.3: Summary of Young's moduli values from microscale tests on cortical bone specimens.

Source	Material	Scale of Microstructure	Test	Young's Modulus in GPa
[45]	Porcine femoral bone	2 μm	Nanoindentation	15
[118]	Human tibial bone	300 μm	Ultrasonic and microtensile testing	18.6
[31]	Bovine tibial bone	1.2 μm	Nanoindentation	13.72
[122]	Human femoral bone	2.8 μm	Nanoindentation	21 - 24
[138]	Bovine tibial bone	2 μm	Nanoindentation	12.9 $\pm$ 2.9
[44]	Human tibial bone	2.8 μm	Nanoindentation	16.6
[130]	Human vertebrae	1 μm	Nanoindentation	18
[62]	Human femoral bone	2.2 μm	Nanoindentation	18-20
[51]	Bovine tibial bone	100 μm	Ultrasonic testing	15

Table 2.4: Summary of the fracture toughness as measured by the stress intensity factors from microscale tests on cortical bone specimens.

Reference	Specimen Type	Orientation of Test	Type of Test	$K_c$in $MPa\sqrt{m}$
[163]	Human femoral bone	Transverse	Three-point bending microscale tests	3 - 8
[79]	Elk antler	Transverse	Three-point bending microscale tests	4-5
[94]	Sheep tibial bone	Longitudinal	Nanoindentation	0.5 - 2

the stress intensity factor has been measured in a few studies, with most researchers utilizing three-point bending tests for small specimens. These results are summarized in Table 2.4.

Bone tissue is particularly unique because the material exhibits toughening mechanisms as a response to applied stresses; these toughening mechanisms have a considerable impact on the fracture behavior of cortical bone. Some of these toughening mechanisms exhibited by bone include microcracking, crack deflection, and fiber bridging [158, 164, 128]. Microcracking, an intrinsic mechanism, redistributes the applied force in a larger area within the material by developing tiny cracks around the point of impact; this behavior results in an increase in fracture resistance as cracks are induced [146, 164, 156, 28, 147, 106, 107]. Crack deflection is an extrinsic mechanism which reorients small cracks to grow in a direction that avoids the creation of even larger cracks [125, 79, 112, 99, 50, 85, 164, 93]. Fiber bridging is a phenomenon where a fiber within the material connects the two shores of a crack, thereby inhibiting further separation [158, 98, 160, 99, 79].

Measurements have been conducted on the mechanical properties of the individual components within bone. On the nanoscopic scale, the Young's modulus of synthetic carbonated apatite is around 109 GPa, and the Young's modulus of a large single

geological carbonated apatite crystal is about 114 GPa [155]. Collagen has a tensile yield strength of 10 - 20 GPa [127]. The mechanical properties of mineralized collagen fibrils, the building block of all bone components, has been examined using tension tests and sonic velocity. These tests produced a Young's modulus ranging from 162 MPa to 825 MPa [155].

The literature also reports Young's moduli in the micro-scale and nano-scale, which are the length scales being studied in the presented research. At a length sale of 2-100μm, the Young's modulus of bone is around 18-22 GPa [120, 119, 121, 51, 167, 166].

2.5 Chapter Summary

The mineralized collagen fibrils, made up of type 1 collagen, carbonated apatite, and water, are the building blocks of bone and contribute to the mechanical properties of interest in the material. These building blocks are arranged in hierarchical structures of different sizes, and the combination of the mechanical properties of these structures produces the high toughness values exhibited by the composite material. The bone can be divided into cortical and trabecular bone, and each type consists of osteons made up of lamella and mineralized collagen fibrils. The properties of these constituents have been investigated in previous papers at both a macroscopic and microscopic scale, and are to be considered when characterizing the fracture processes within bone.

CHAPTER 3 MATERIALS

The purpose of the research presented in this thesis is to characterize fracture in cortical bone tissue using novel methods of small-scale mechanical testing such as micro-scratch tests and nanoindentation. To experimentally understand the processes involved in fracture in bone, specimens must be chosen and prepared in a manner that accurately portrays the hierarchical nature of bone, and samples must be developed in a consistent and reproducible manner. These specimens must be harvested in a fashion that protects the integrity of the bone tissue, and the samples must be prepared using specialized equipment that are capable of protecting the bone specimens from contamination. The purpose of the preparation techniques detailed in this chapter is to expose a surface on the bone that visually showcases the constituent structures within the bone, as well as any observable failure mechanisms after mechanical testing is completed.

3.1 Specimens

The research on characterizing the fracture properties of bone requires experimental data from multiscale mechanical testing of bone samples. This study is focused on porcine and bovine bone specimens cut in the longitudinal direction and tested in the transverse direction. The porcine bone specimens are harvested 24 hours after slaughter from 22-26 week old animals. The animals had a corn diet and were purchased from the University of Illinois Meat Science Laboratory. The bovine bone specimens are purchased from the L&M Slaughterhouse in Georgetown, Illinois. The femoral bones are sealed in a plastic airtight bag and frozen at -20^oC until retrieved. Previous research suggests that there is a 10% decrease in stiffness and unloading energy and a 10% increase in loss tangent between reported mechanical property values for 2 and

24-hour post-mortem bone specimens [82]. The focus of the presented research is to generate a method to assess the mechanical performance at the microscopic scale. For purposes of convenience, the research focuses on ex-vivo testing.

The specimens are extracted from the cross-section of the mid-diaphysis of the femoral bone as displayed in Figure 3.1. This part of the bone has been chosen specifically for this research; previous investigations have suggested that the cross-section of femurs and other long bones feature a dense shell of cortical bone around a trabecular interior [119]. The dense cortical bone tissue at the femur provides a large and consistent surface area to prepare and test.

3.2 Laboratory Equipment

Cutting, grinding, and polishing are essential preparatory techniques utilized in the creation of specimens that can be tested for a large variety of experimental procedures involving the investigation of material mechanical properties. For the procedure of cutting the thawed porcine femoral bone, a Gryphon Corp C-40 table-top band saw as shown in Figure 3.2 is available to section the bone into smaller, manageable pieces. The table-top band saw is lubricated with water, and should be used without gloves to minimize the chances of encountering the rapidly moving blade.

After the embedment procedure, a Buehler IsoMet 5000® Linear Precision Saw as shown in Figure 3.3 is available for sectioning the embedded specimens of porcine femoral bone. The instrument is equipped with a 2-μm precision cut alignment, automatic dressing system for optimal blade maintenance, a clear safety hood for viewing specimens, and the SmartCut® system for preventing overheating in specimen being cut and in the instrument. The sample is attached to the saw using a variety of clamps; the clamp needed is determined by the researcher on the basis of how large

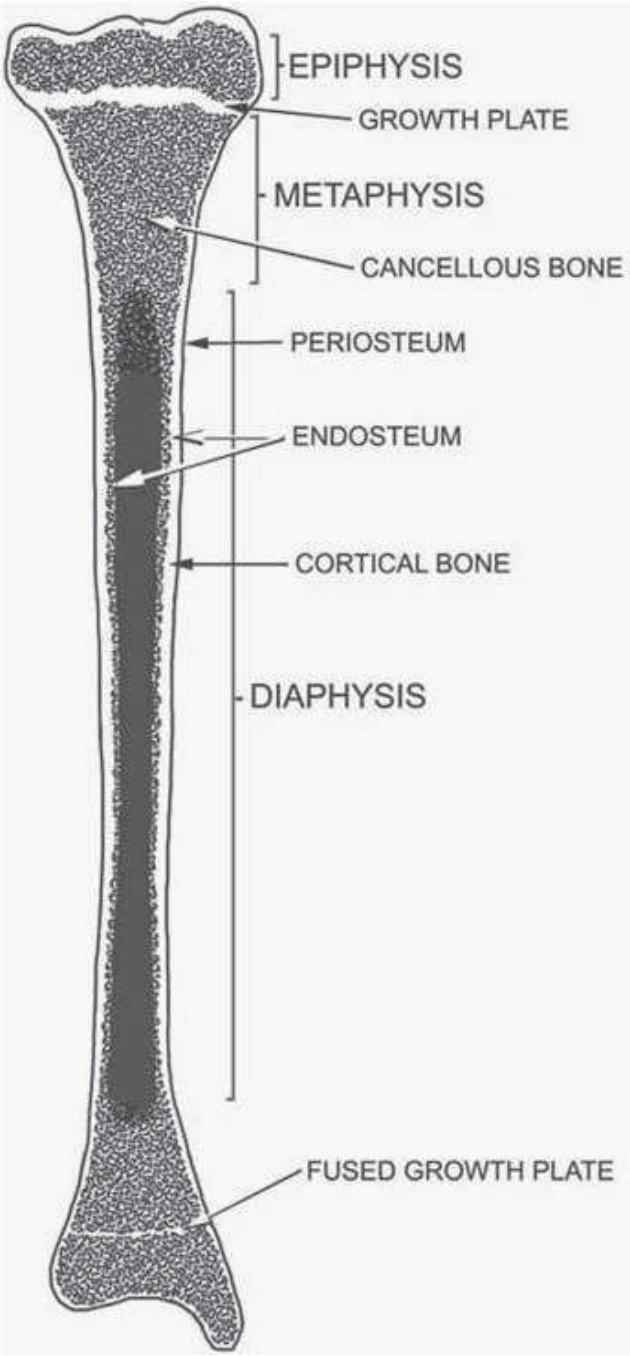

Figure 3.1: Parts of a femoral bone (from [6]).

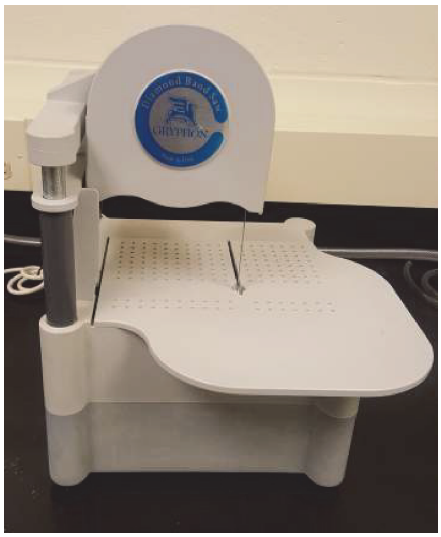

Figure 3.2: Gryphon Corp C-40® table band saw used for sectioning the bone.

and irregularly shaped the sample is. After the sample is placed in the saw, settings such as the thickness of the sample, how deep the blade should cut, and blade speed are input into the specialized saw and the cutting cycle is initialized. Because of the nuances surrounding the use of this machine, it is imperative to consult the user's manual before and during each use.

Depending on the sample material, the specimen may need to be dried using the Memmert UF 55® laboratory vacuum oven available in the laboratory to remove the excess moisture from the specimen due to the lubricant used in the cutting procedure, and then placed in a vacuum dessicator until the researcher is ready to grind and polish.

For the procedure of polishing, a Buehler EcoMet 250/AutoMet 300® Grinder-Polisher instrument as shown in Figure 3.4 is available for use in the laboratory. The instrument is equipped with a variable speed power head for complementary and contra rotation, and is easy to clean and operate. The procedure for using the grinder-polisher involves the selection of a grinder pad, which comes in different grit

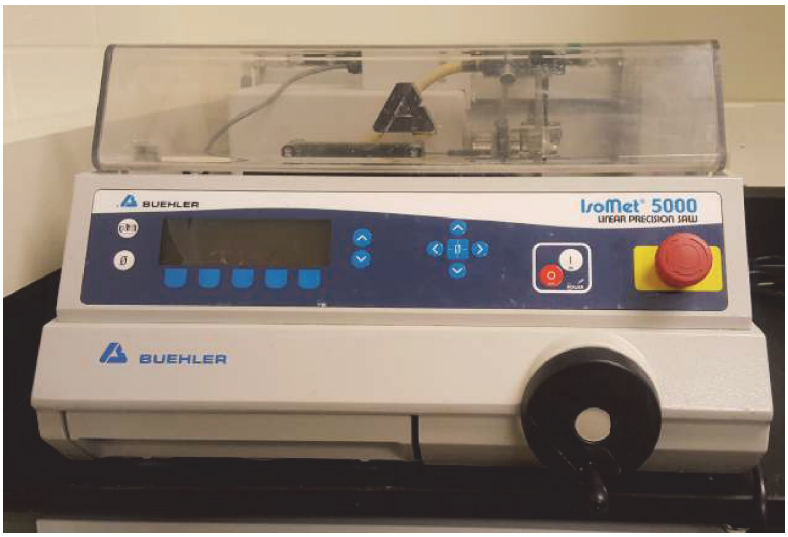

Figure 3.3: Buehler IsoMet 5000® Linear Precision Saw used to section embedded specimens into 5-mm samples.

sizes. The rule of thumb is to start at a low grit and run the machine for a short amount of time of about fifteen seconds under a lower force to check on the health of the specimen. Settings such as the time to run the grinding or polishing procedure, the speed of the base and head of the machine, the direction in which the base and head spin, and the force used during the procedure should be input first before the sample is placed in the head. Pressing the two green buttons on the side of the head should lower the head to the base, and pressing the buttons again should begin the test. It is imperative to use a mild lubricant like deionized water on biological materials like bone during the grinding procedure.

After each grinding or polishing procedure, the sample should be inspected visually under light after the excess lubricant has been blow-dried, and then cleaned ultrasonically. For the procedure of cleaning, a Branson 5800® Ultrasonic Cleaner as shown in Figure 3.5 is available for use in the laboratory. The procedure for using the cleaning bath involves selecting a solvent like deionized water and placing

Figure 3.4: Buehler EcoMet 250/AutoMet 300® Grinder-Polisher instrument.

the specimen into a beaker containing the solvent. The beaker is then held partially submerged in the bath while the sonic cleaning setting is used to thoroughly clean the sample for a specified amount of time. The sample can be qualitatively inspected using the available optical microscope to see just how polished the specimen is.

Finally, a Marvel Scientific 6CRF® refrigerator is available for storage at temperatures below room temperature in the laboratory.

3.3 Chapter Summary

This chapter reveals that the source of the porcine and bovine femoral bone specimens used in the presented research is the Meat Science Laboratory at the University of Illinois Department of Animal Science. The chapter also presents the instruments available for preparing specimens in the Sustainability under the Nanoscope Laboratory at the University of Illinois at Urbana Champaign.

The instruments and their purposes are outlined below

Figure 3.5: Branson 5800® Ultrasonic Cleaner.

- Gryphon Corp C-40® table-top band saw – for sectioning the bone into smaller pieces.
- Buehler IsoMet 5000 Linear Precision saw® – for cutting the embedded bone specimens into 5-mm samples.
- Buehler EcoMet 250/AutoMet 300 Grinder-Polisher® – for grinding and polishing the bone surface.
- Branson 5800 Ultrasonic Cleaner® – for cleaning the sample ultrasonically between grinding and polishing steps.
- Marvel Scientific 6CRF refrigerator® – for storing the bone at temperatures below room temperature.

These specialized instruments are referenced in the following chapter detailing the specimen preparation procedure.

CHAPTER 4 SPECIMEN PREPARATION

To adequately investigate the fracture processes within bone, the specimens must be prepared in a way that aids visualization of the relevant constituent components of bone tissue through microscopy, and provides a space on the specimen that is suitable for testing. This chapter outlines the procedure used to polish the specimens to reveal the osteons, and details the methods used to preserve specimens before, during, and after preparation. The significance of having a process that yields consistent specimens is integral to producing rational results while testing such a variable material like cortical bone.

4.1 Initial Sample Preparation

Porcine femoral bones were acquired from the Meat Science Laboratory at the Department of Animal Sciences in the University of Illinois at Urbana-Champaign. Bovine femur bones were acquired from L&M Slaughterhouse in Georgetown, IL. The cortical bone specimens, an example of which is shown in Figure 4.1, were frozen at -20^oC before any sample preparation procedures were performed. The samples were frozen as a requirement to ensure that the delicate material is kept fresh and contamination-free, and to reduce the impact of the post-mortem process on the mechanical properties of the bone, a phenomena catalogued through compliance investigations [48]. Linde et al [82] discussed the effects of different storage methods on the mechanical properties of bone; the study conducted on trabecular bone determined that the gain in stiffness due to freezing can be ignored for being statistically insignificant. Therefore, the presented research assumes that storage while frozen does not impact the integrity of the denser cortical bone specimens.

The samples were thawed in cold water for an hour, and the mid-diaphysis of the

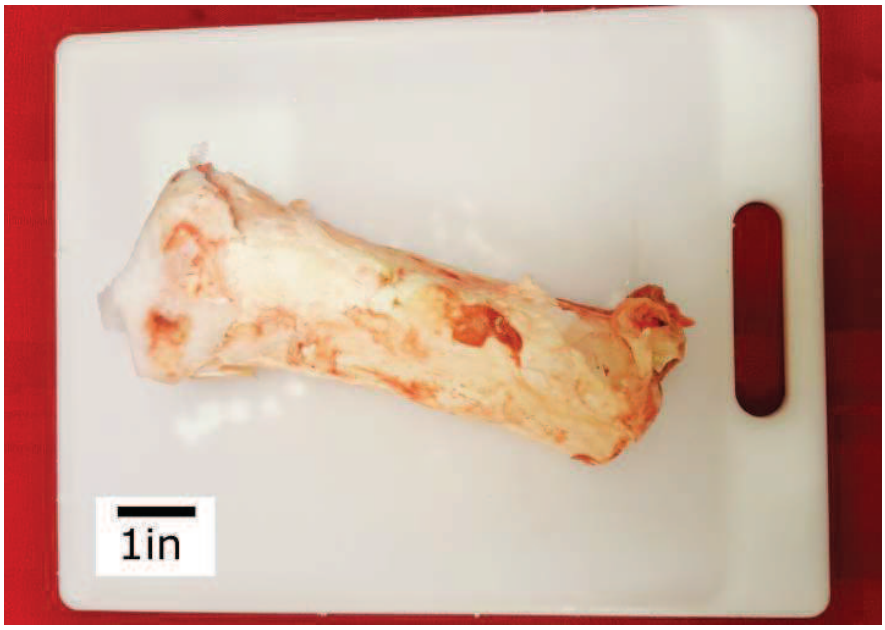

Figure 4.1: Frozen porcine femoral bone.

femoral bone was divided into smaller sections with a band saw. The line of cutting is perpendicular to the major axis of the femoral diaphysis to expose a longitudinal surface section of the cortical bone. To reveal the cortical bone, the muscle and trabecular bone tissues were gently removed using a medical dissection kit. Previous research has discovered that the processes of thawing and refreezing do not significantly impact the characteristic properties of the material observed during mechanical testing [82], therefore the remaining femoral bone is frozen and stored at -20^oC until further sectioning is needed to make new samples.

The smaller sections of cortical bone were cleaned ultrasonically in a solution consisting of 1000-ml of deionized water, 50-ml of household bleach, and 15-ml of Alconox cleaning detergent for 20 minutes. After ultrasonic cleaning, the cortical bone specimens were embedded in a poly(methyl methacrylate) or PMMA epoxy. The research began with the utilization of Buehler Epothin 2® epoxy system. The

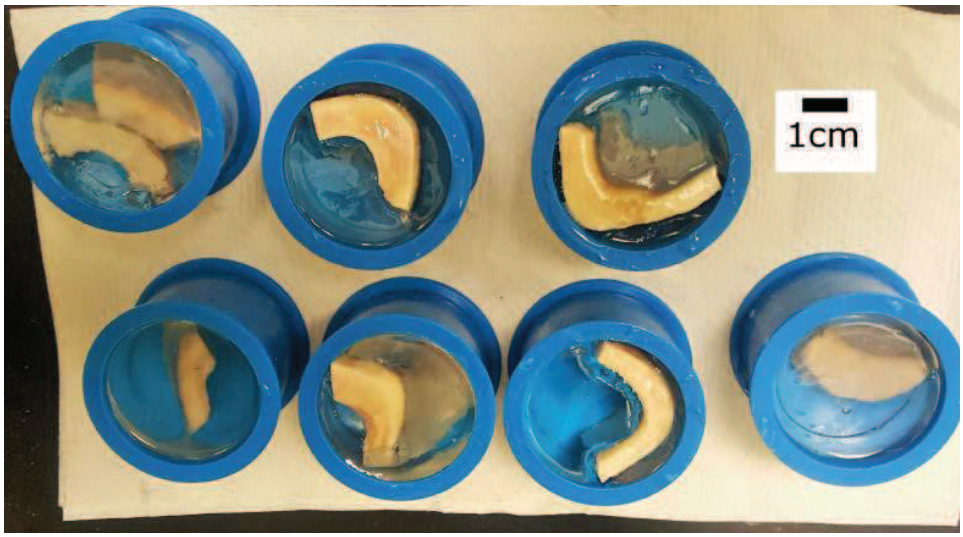

Figure 4.2: Cortical bone specimens embedded in PMMA after being ultrasonically cleaned.

system was replaced with PMMA because the epoxy system created a composite-like sample by filling all voids within the porous bone tissue. The embedment process requires the use of cylindrical molds with a 1-inch diameter to facilitate an easier cutting and polishing process, as the shape of the molds fits easily in the instruments used in the laboratory and described in Chapter 3. The freshly cleaned cortical bone specimens were placed at the bottom of the plastic mold before the PMMA mixture is carefully poured. The hardening process can take as long as 24 hours before the specimens are ready for demolding and further cutting. Freshly embedded specimens are shown in Figure 4.2.

The embedded cortical bone samples were cut using the precision saw described in Chapter 3, fitted with IsoCut Wafering Blades® with an arbor size of 12.7 mm and a thickness of 0.889 mm. The precision saw utilizes Buehler IsoCut fluid as a lubricant during the cutting process to reduce the effects of friction and heat upon the surface of the cortical bone. The instrument is programmed to cut samples into

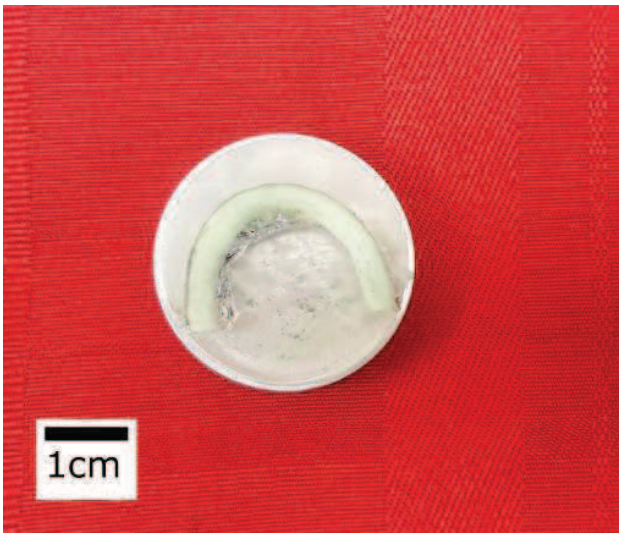

Figure 4.3: Specimen mounted on 32-mm aluminum disk.

5-mm specimens with a blade speed of 1500 rpm at a rate of 2.5 mm per minute. A lower rate is needed to ensure that the blade passes through the specimen without curving, thereby producing flat specimens. The cut cortical bone specimens are then mounted on 32-mm diameter aluminum disks using cyanoacrylate glue to add some necessary stability during the grinding and polishing process. A mounted specimen is displayed in Figure 4.3.

4.2 Previous Grinding and Polishing Protocols

The grinding and polishing procedure went through a few iterations before the finalization of the preparation procedure. The first trial, named Protocol 1, consisted of grinding the sample on 400-, 600-, 800-, and 1200-grit silicon carbide abrasive pads for 2 minutes each under a load of 2 lbs. The specimens were then polished using 9-μm, 3-μm, 1-μm, and 0.25-μm polishing suspension fluids for 15 minutes under a load of 3 lbs. Each polishing step used a base speed of 300 rpm and a head speed of 60 rpm on the Ecomet/Automet Grinder-Polisher. The specimens were cleaned ultra-

Table 4.1: Protocol 1 Grinding Procedure.

Step	Grit Size	Pad Type	Base Speed	Head Speed	Duration	Force
1	400-grit	Silicon carbide	300 rpm	60 rpm	2 minutes	2 lb
2	600-grit	Silicon carbide	300 rpm	60 rpm	2 minutes	2 lb
3	800-grit	MicroCut®	300 rpm	60 rpm	2 minutes	2 lb
4	1200-grit	MicroCut®	300 rpm	60 rpm	2 minutes	2 lb

Table 4.2: Protocol 1 Polishing Procedure.

Step	Particle Size	Pad	Base Speed	Head Speed	Duration	Force
1	9-microns	TexMet P®	300 rpm	60 rpm	15 minutes	3 lbs
2	3-microns	TexMet P®	300 rpm	60 rpm	15 minutes	3 lbs
3	1-micron	TexMet P®	300 rpm	60 rpm	15 minutes	3 lbs
4	0.25-microns	TexMet P®	300 rpm	60 rpm	15 minutes	2 lbs
5	0.05-microns	MicroCloth®	300 rpm	60 rpm	4 minutes	2 lbs

sonically between steps for 2 minutes. This first attempted procedure, summarized in Table 4.1 and Table 4.2, yielded observable osteons under the microscope, but the specimens exhibited deep scratches on the surface. To buff out the deep scratches, a polishing cycle on a microcloth pad for 4 minutes under a load of 3 lbs was introduced into the procedure. The effects of this first protocol can be viewed in Figure 4.4.

After an extensive literature review, a faster procedure named Protocol 2 was developed and tried on the cortical bone specimens. The specimens were ground using 400-, 600-, 800- and 1200-grit silicon carbide pads for 2 minutes each under a

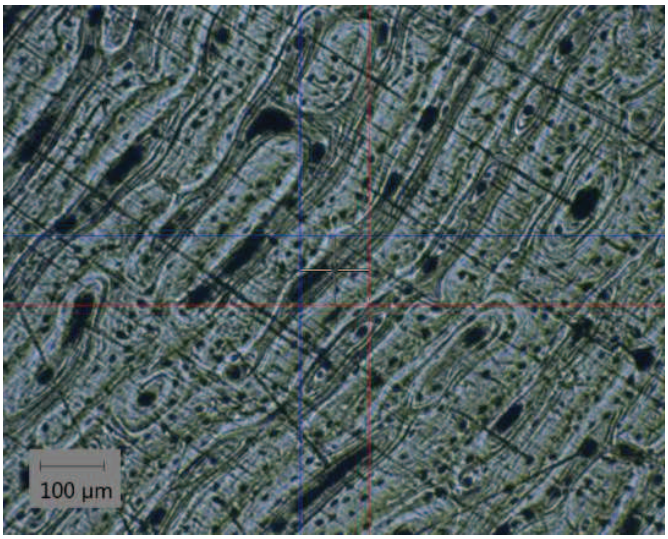

Figure 4.4: Cortical bone prepared using Protocol 1 displaying deep scratches.

load of 2 lbs. The specimens were then polished on a microcloth pad for 4 minutes under a duration of 3 lbs with a 0.05-μm polishing suspension fluid. This procedure, summarized in Table 4.3 and Table 4.4, also yielded deep scratches on each sample, and the surfaces were not consistently smooth. Furthermore, the samples were often wedged and uneven. The effects of the second trial procedure can be seen in Figure 4.5.

Longer grinding and polishing times are necessary to avoid deep scratches and to provide a more uniform and smooth surface. Protocol 3 was developed for this purpose, and is summarized in Table 4.5 and Table 4.6 . The specimens were ground on the 400-grit pad for 1 minute, the 600-grit pad for 5 minutes, and the 800- and 1200-grit pads for 15 minutes each; all grinding cycles were conducted under a constant load of 2 lbs. The polishing procedure required 3-μm, 2-μm, and 0.25-μm polishing suspension fluids on Buehler TexMet P® pads, and 0.05-μm polishing suspension on a Buehler MicroCloth® pad; each cycle lasted for 20 minutes under a load of 2 lbs. This new procedure yielded a shiny and smooth surface on the specimens, but did

Table 4.3: Protocol 2 Grinding Procedure.

Step	Grit Size	Pad Type	Base Speed	Head Speed	Duration	Force
1	400-grit	Silicon carbide	300 rpm	60 rpm	2 minutes	2 lb
2	600-grit	Silicon carbide	300 rpm	60 rpm	2 minutes	2 lb
3	800-grit	MicroCut®	300 rpm	60 rpm	2 minutes	2 lb
4	1200-grit	MicroCut®	300 rpm	60 rpm	2 minutes	2 lb

Table 4.4: Protocol 2 Polishing Procedure.

Step	Particle Size	Pad	Base Speed	Head Speed	Duration	Force
1	0.05-microns	MicroCloth®	300 rpm	60 rpm	4 minutes	3 lbs

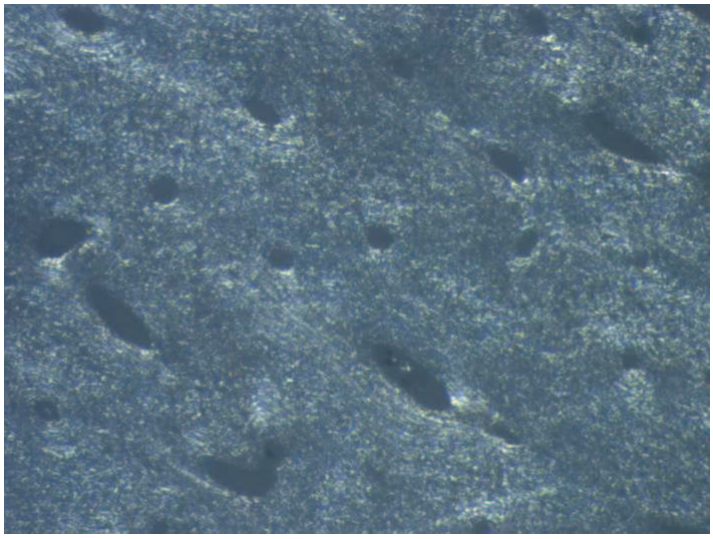

Figure 4.5: Cortical bone prepared using Protocol 2 displaying a rough surface with osteonal boundaries barely visible.

Table 4.5: Protocol 3 Grinding Procedure.

Step	Grit Size	Pad Type	Base Speed	Head Speed	Duration	Force
1	400-grit	Silicon carbide	300 rpm	60 rpm	1 minute	2 lb
2	600-grit	Silicon carbide	300 rpm	60 rpm	5 minutes	2 lb
3	800-grit	MicroCut®	300 rpm	60 rpm	15 minutes	2 lb
4	1200-grit	MicroCut®	300 rpm	60 rpm	15 minutes	2 lb

Table 4.6: Protocol 3 Polishing Procedure.

Step	Particle Size	Pad	Base Speed	Head Speed	Duration	Force
1	3-microns	TexMet P®	300 rpm	60 rpm	20 minutes	2 lbs
2	1-micron	TexMet P®	300 rpm	60 rpm	20 minutes	2 lbs
3	0.25-microns	TexMet P®	300 rpm	60 rpm	20 minutes	2 lbs
4	0.05-microns	MicroCloth®	300 rpm	60 rpm	20 minutes	2 lbs

nothing to rectify the unevenness in the samples. To fix the issue, a lower applied force and speed was substituted for instrument grinding in the 400 and 600 grit cycles. The sample is then checked every 30 seconds during the 400-grit and 600-grit grinding steps to ensure the integrity and flatness of the cortical bone sample.

4.3 Final Grinding and Polishing Procedure

The grinding procedure for cortical bone is designed to expose a flat surface of osteons to observe and test. Specimens are ground using abrasive discs of successively smaller grit sizes until the constituent osteons can be imaged using optical microscopy.

The procedure was performed on a Buehler Ecomet/Automet 250® semi-automatic grinder and polisher. The first step required grinding the specimens on a 400-grit Buehler Carbimet® silicon carbide pad for 1 minute using a force of 1 lb. The base speed of the instrument was set to 100 rpm and the head speed was set to 60 rpm. The next step required grinding on a 600-grit Buehler Carbimet® silicon carbide pad for 5 minutes with a force of 1 lb; the base speed was increased to 150 rpm and the head speed was kept stable at 60 rpm. The specimens were then ground on 800-and 1200-grit Buehler MicroCut® silicon carbide pads for 15 minutes each. The base speed and head speed were maintained at 150 rpm and 60 rpm respectively, and the instrument was set to use a force of 1 lb.

Polishing the samples improves upon the grinding process by exposing a reflective surface to facilitate better optical microscopy images. Additionally, polishing creates an even and clean surface on which tests are performed. The procedure was also performed on a Buehler Ecomet/Automet 250® instrument. Specimens were polished on Buehler TexMet P® pads using 3-μm, 1-μm, and 0.25-μm polishing suspension fluid successively. Each step was performed for 20 minutes under a load of 2 lbs, with the head speed maintained at 60 rpm but the base speed increased to 300 rpm. The specimens were then polished on a Buehler MicroCloth® pad using a 0.05-μm polishing suspension fluid, also for 20 minutes under a load of 2 lbs. The base and head speeds remained the same at 300 rpm and 60 rpm respectively.

Between each successive grinding and polishing step, the specimens were cleaned ultrasonically for 2 minutes using a Branson 5800® Ultrasonic cleaner. A summary of the grinding and polishing steps is shown in Table 4.7 and 4.8.

The procedure outlined in this section expose a virgin and smooth surface of the bone. The osteons are observable using optical microscopy at a magnification of 5x and 20x, as shown in Figure 4.6 and Figure 4.7.

Table 4.7: Finalized Grinding Procedure.

Step	Grit Size	Pad Type	Base Speed	Head Speed	Duration	Force
1	400-grit	Silicon carbide	100 rpm	60 rpm	1 minute	1 lb
2	600-grit	Silicon carbide	150 rpm	60 rpm	5 minutes	1 lb
3	800-grit	MicroCut®	150 rpm	60 rpm	15 minutes	1 lb
4	1200-grit	MicroCut®	150 rpm	60 rpm	15 minutes	1 lb

Table 4.8: Finalized Polishing Procedure.

Step	Particle Size	Pad	Base Speed	Head Speed	Duration	Force
1	3-microns	TexMet P®	300 rpm	60 rpm	20 minutes	2 lbs
2	1-micron	TexMet P®	300 rpm	60 rpm	20 minutes	2 lbs
3	0.25-microns	TexMet P®	300 rpm	60 rpm	20 minutes	2 lbs
4	0.05-microns	MicroCloth®	300 rpm	60 rpm	20 minutes	2 lbs

Figure 4.6: Optical microscopy of polished cortical bone specimens at a magnification scale of 5x.

(a) Optical microscopy of porcine cortical bone.

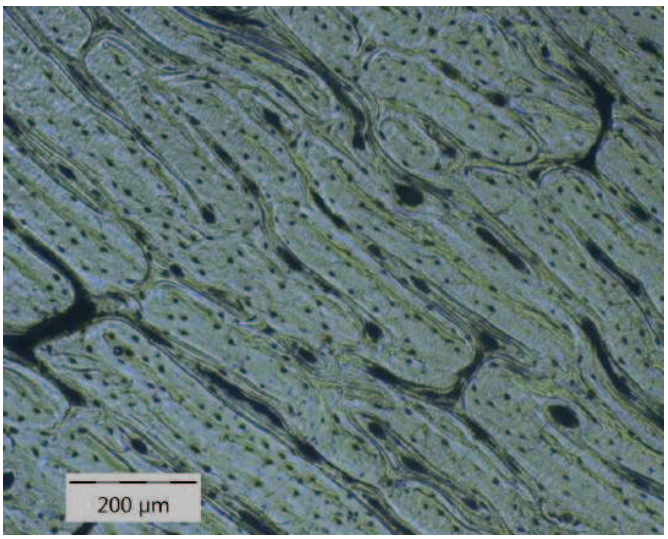

(b) Optical microscopy of bovine cortical bone.

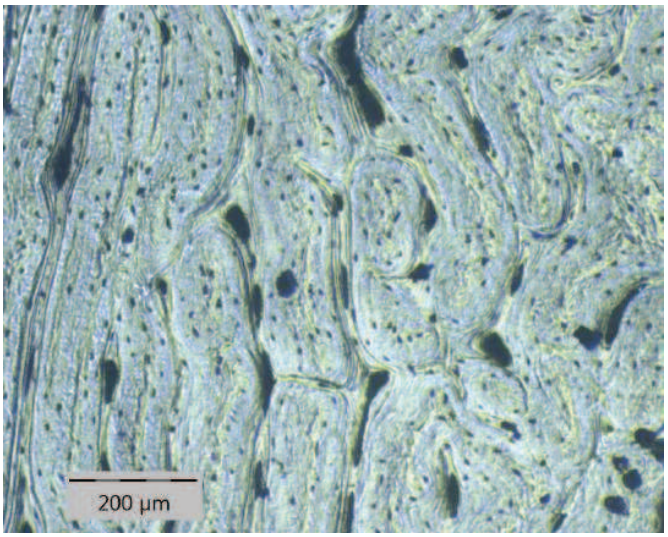

Figure 4.7: Optical microscopy of polished cortical bone specimens at a magnification scale of 20x.

(a) Optical microscopy of porcine bone.

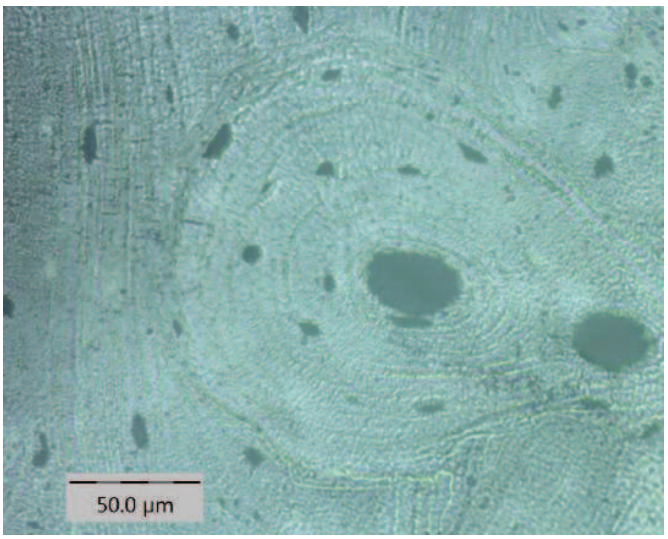

(b) Optical microscopy of bovine bone.

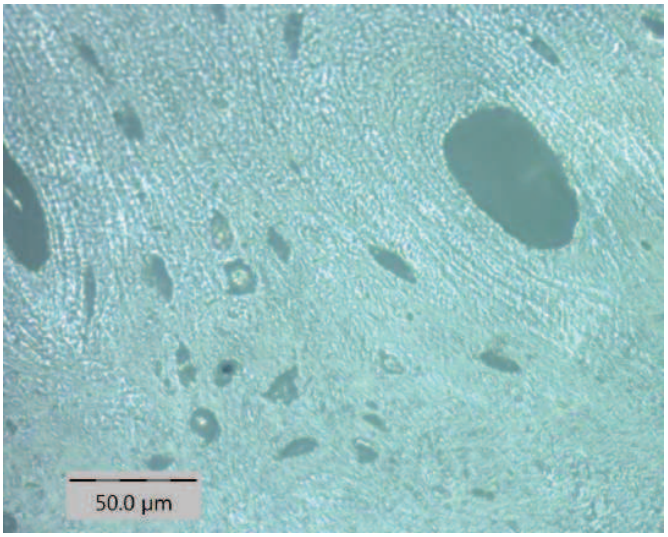

4.4 Sample Storage

Because refreezing, thawing, and retesting multiple times did not alter the mechanical properties of the bone specimen significantly in previous studies [82], the porcine and bovine femurs were stored at -20^oC before sample preparation, and at 4^oC between preparation steps. For scratch tests, the bone specimens were wrapped in gauze soaked in Hanks' Balanced Salt Solution (HBSS) before and after embedment. The samples were kept wrapped in the gauze after the grinding and polishing procedure until testing. For indentation tests, the bone specimens were dried in a Memmert UF 55 laboratory vacuum oven laboratory oven for 24 hours at 50^oC before the embedment process begins. After the specimens have been embedded, the samples were kept under vacuum in a desiccator until testing. After testing, specimens were also kept under vacuum in a desiccator until the scratches are imaged using a Scanning Electron Microscope.

4.5 Chapter Summary

This chapter explores the sample preparation aspect of the experimentation presented in the thesis by describing the intricate grinding, polishing, and cleaning procedure developed to prepare porcine and bovine cortical bone specimens. The chapter describes the initial procedures attempted on the cortical bone specimens, and the steps taken to improve the final polish of the specimens. This chapter also describes the procedures developed to store the specimens in a proper manner that deters deterioration of the bone. The presented procedures in this chapter are with respect to the specialized equipment available in the Sustainability Under the Nanoscope Laboratory at the University of Illinois at Urbana-Champaign.

CHAPTER 5 NANOINDENTATION

Because of the limited amount of specimens available for testing purposes, a method must be devised that can yield several results from a single specimen. Furthermore, the experiment must be able to accurately distinguish between the mechanical properties of the constituent materials within the complex and hierarchical structure of bone. Because the hierarchical structure is important in investigating cracks at different length scales, the scale of the crack determines the affected structures and fracture mechanisms involved in analyzing the results [97]. Therefore, in an investigation of the microscopic and nanoscopic mechanical properties within bone, bulk tensile and compressive tests are inadequate for a detailed study; the presented research develops an experimental protocol based on a technique known as nanoindentation. The results from the nanoindentation test are based upon the Oliver-Pharr mathematical model which yields the hardness and the elastic modulus of cortical bone.

5.1 Introduction to Nanoindentation

Nanoindentation tests are an advanced mechanical testing procedure based upon the idea of pushing a probe made of a material of known mechanical properties into a softer material made of unknown mechanical properties. The interaction between the two materials based upon the load used in the experiment and the resulting displacement provides an insight into the softer material's mechanical properties. The technique can be traced back to primitive material investigation techniques developed by man; humans have always tested the relative hardness of an unknown substance by placing it in contact with a known material. Other tests have been developed using the same fundamental theory; including the Meyer hardness test which is based upon the projected area of the probe's impression upon a material, and the Brinell scale,

which is based on one of the first tests developed using a standardized large indenter [137, 13, 81]. Nanoindentation technology has developed to continously measure load and displacement during the indentation experiment [81]. Presently, nanoindentation is used in the determination of mechanical properties such as fracture toughness, hardness, and elastic moduli in a variety of materials such as nanometer-thick films [81, 114, 55, 101, 80], polymers [21, 83, 145, 108], silicon [41, 161], and metal alloys [75, 7, 139].

The importance of nanoindentation in the research presented in this thesis is based upon the complexity of bone, and the different structural-mechanical functions of the constituent components that make up the hierarchical structure of the material. Therefore, a reproducible and consistent experimental method is needed to determined mechanical properties of bone on a submicron scale, and this information can be obtained in a conservative and sustainable manner using probing techniques.

5.2 Theory of Nanoindentation

The general framework procedure for determining mechanical properties of materials through nanoindentation can be attributed to the work introduced by W. C. Oliver and G. M. Pharr [111, 110, 84, 139, 15, 115, 114, 113, 140, 70, 63]. The referenced papers introduce and expand the concept of nanoindentation by describing it as a technique based upon the elastic contact problem, which was developed originally by three pioneers of contact mechanics - Joseph Valentin Boussinesq, a French mathematician who developed some of the first theories on solid elastic mechanics [20], Heinrich Hertz, a German physicist who pioneered the combination of geometry and kinematics [64], and Ian Naismith Sneddon, a Scottish mathematician who expanded on the basis of contact mechanics and elasticity in “punching” impacts [53, 133, 134].

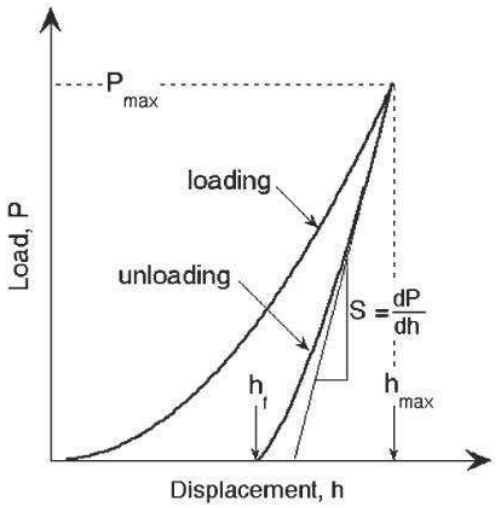

Figure 5.1: Typical load displacement diagram (from [110]).

Oliver and Pharr associate the computation of the stresses and displacements in an elastic body that is loaded by a rigid indenter to Boussinesq, and reference the work Hertz completed which compared the elastic contact between two spherical surfaces with different radii and elastic constants [111].

The method introduced by Oliver and Pharr in their research articles constitutes the basis of most modern material characterization experiments utilizing the advanced and efficient method of nanoindentation. Due to the advent of load- and depth-sensing indentation methods, nanoindentation can measure important material mechanical properties such as the reduced elastic modulus E_r and the sample hardness H, and these mechanical properties are based upon definitions determined from the Oliver and Pharr mathematical model [46]. The Oliver and Pharr method determines a material's hardness and elastic modulus from indentation load-displacement data. The elastic modulus E and the hardness H are commonly obtained from a cycle of loading and unloading as shown in Figure 5.1; the unloading data is analyzed by concentrating on the contact area measured at peak load [111].

The hardness obtained from nanoindentation is particularly important because the measured hardness resulting from low penetration depths is different from the bulk hardness of the material as a whole, and the distinction is especially important when characterizing bone's hierarchical structure [14]. Furthermore, because nanoindentation is effective in determining the mechanical properties of materials at a submicron scale, nanoindentation can be used to map the properties of a material on a spatially resolved basis [44].

The method of determining mechanical properties from the load-displacement data is dependent on the resulting contact area as the indenter and the subject material interact. Nanoindentation as a way to measure mechanical properties was first attempted using spherical and conical indenter geometries to investigate metallic material. These initial experiments, conducted by D. Tabor [137] and N. A. Stillwell [136], resulted in the idea that plasticity can be accounted for in the analysis of the elastic unloading data by characterizing the shape of the indented surface or the contact area, which is determined from the indenter shape function [111]. This dependence is based upon the educated assumption that the material being indented reshapes itself around the indenter as a function of the depth, and if the shape function of the indenter is known, the area of contact can therefore be calculated [111].

In a subsequent paper published in 2004, Oliver and Pharr suggest that the relationship between the loading, displacements and contact area can be represented by describing the mechanics of the punching action as a paraboloid of revolution of a smooth function [110]. The load displacement relationship of a particular punch geometry can be written as:

$$P = \alpha h^m$$

where P represents the indenter load, h represents the indenter's elastic displace-

ment, and α and m are constants corresponding to the geometry of the indenter being used [111, 110]. Three important values are obtained experimentally from the load-displacement curves; these three properties include P_{max}, which represents the maximum load, h_{max}, which represents the maximum displacement, and the elastic unloading stiffness, $S = dP/dh$. The unloading stiffness is related to the elastic modulus of the material and the contact area with the following formula:

$$S = \frac{dP}{dh} = \frac{2}{\sqrt{\pi}} E_r \sqrt{A}$$

where $S = dP/dh$ is the stiffness of the upper portion of the unloading data measured through experimentation, E_r is the reduced modulus, and A is the projected area of elastic contact [111, 110].

The hardness can then be determined as follows:

$$H = \frac{P_{max}}{A}$$

where P_{max} is the peak indentation load and A is the projected area of the hardness impression [111, 110].

5.3 Theory of Statistical Nanoindentation

Because bone is a heterogeneous material with a range of mineralization levels and collagen protein content within the osteons on a micro- and nano-scale, nanoindentation must be applied over an area to statistically represent the measured mechanical properties of the material within an appropriately chosen grid and indentation depth that corresponds to the length-scale of interest, and can capture the phases within the heterogeneous material. The results from the nanoindentations over the chosen

area must undergo a statistical deconvolution to resolve the mechanical properties into their respective phases. The model for statistical deconvolution is predicated on the assumption that there are two phases of sufficient contrast in any tested area within the bone specimen; this model was developed by Ulm et al, is presented below [135, 141, 90, 142, 35, 144].

The distribution of the mechanical properties of indentation modulus M and hardness H of each phase J can be represented as a Gaussian distribution as follows:

$$p_j(x) = \frac{1}{\sqrt{2\pi s_J^2}} \exp\left(-\frac{(x-\mu_J)^2}{2s_J^2}\right),$$

where μ_J is the arithmetic mean of the mechanical property in question as defined by N_J and s_J is the standard deviation. The mean and the standard deviation can be determined as follows:

$$\mu_J = \frac{1}{N_J}\sum_{k-1}^{N_J} x_k, \quad s_J^2 = \frac{1}{N_J - 1}\sum_{k-1}^{N_J}(x_k - \mu_J)^2$$

In the case of a heterogeneous material with two or more phases, the frequency distribution of the mechanical properties adheres to the following theoretical probability density function:

$$P(x) = \sum_{J-1}^{n} f_J p_J(x),$$

where $f_J = N_J/N$ is the surface fraction occupied by phase J subject to the constraint:

$$\sum_{J-1}^{n} f_J = 1$$

The statistical deconvolution yields the mean and standard deviation of the nanoindentation modulus and hardness, as well as the surface fraction for each mechanical phase.

5.4 Nanoindentation Testing Instrument

After the sample preparation procedure is completed, the specimen undergoes nanoindentation using an NHT2 Nanoindentation Tester platform shown in Figure 5.2. The platform is designed by CSM Instruments, an Anton Paar division. The NHT2 module as displayed in Figure 5.3 is fitted with a Berkovich diamond indenter and is attached to an optical microscopy instrument. The software records the hardness and elastic modulus for each indent. The instrument delivers a maximum force of 500 mN, and includes a reference ring as shown in Figure 5.4 to provide constant measurement of the amount of penetration made into the specimen being indented. The high precision load and displacement measurements are collected with a capacitive sensor and a precision electromagnetic coil, as displayed in Figure 5.4. The technical details for the loading and penetration depth ranges are listed in Table 5.1 and Table 5.2 respectively.

The Berkovich tip is a three-sided pyramidal indenter probe with a semi-vertical angle of 65.3^o. The contact area at peak load is dependent on the indenter geometry and the contact depth; the indenter geometry can be described by an area function $F(h)$ where h is the contact depth. The area function for a perfect Berkovich indenter is as follows [54, 47]:

$$A_T = \pi h_c^2 \tan^2 \varphi = \kappa h_c^2$$

where $\varphi = 70.32^o$and $\kappa = 24.56$.

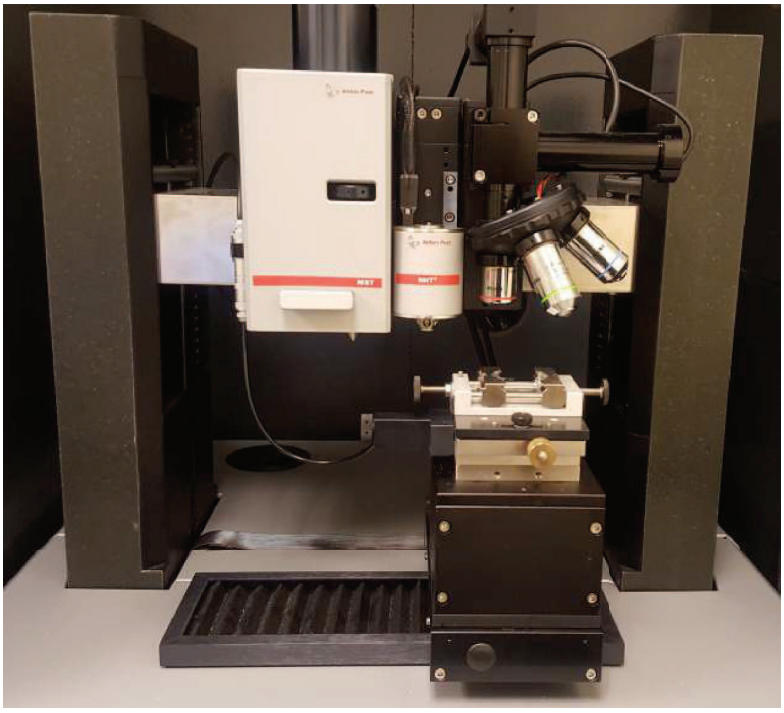

Figure 5.2: Nanoindentation and Micro-scratch tester configuration with attached optical microscope.

Figure 5.3: NHT2 Module (from Anton Paar Nanoindentation tester NHT2 Technical Features Brochure).

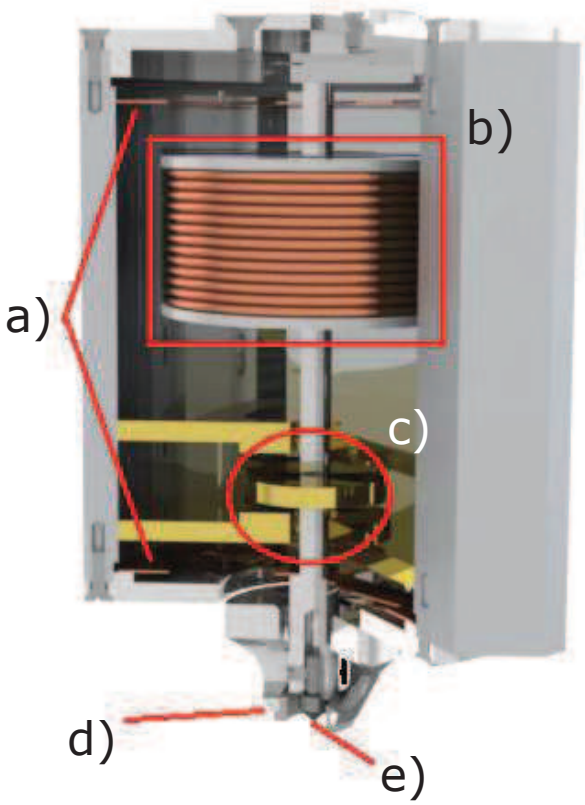

Figure 5.4: Cross-section of NHT2 module: a) Springs to ensure vertical movement of the indenter. b) Electromagnetic coil to control displacement. c) Capacitive sensor to record displacement of the indenter. d) Reference ring. e) Diamond indenter. (from Anton Paar Nanoindentation tester NHT2 Technical Features Brochure).

Figure 5.5: Indenter approach schematics (from Anton Paar Nanoindentation tester NHT2 Technical Features Brochure).

(a) Initial Setup. (b) Final approach of indenter.

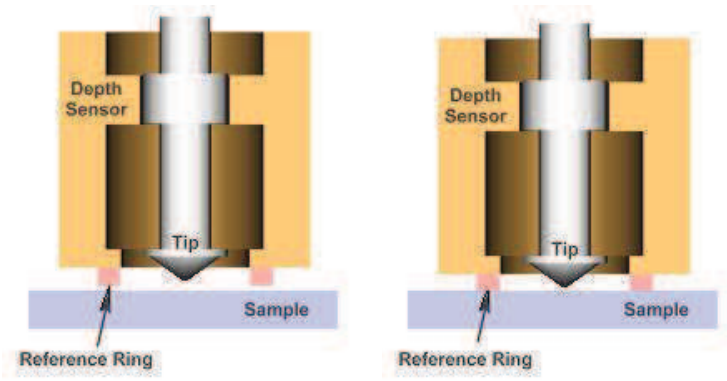

Table 5.1: Normal load technical specifications. (from Anton Paar Nanoindentation tester NHT2 Technical Features Brochure).

	Fine Range	Large Range
Maximum indentation loadF_{max} in mN	30	500
Load resolution in nN	20	300
Noise Floor inμN	1	
Normal load range of indentation in mN	0.1 to 500	
Minimum usable load F_{max} in mN	0.1	
Minimum contact force in μN	Less than 1	
Loading rate in mN/min	Up to 10000	
Frame stiffness in N/m	10^7	
Contact force hold time	unlimited	

Table 5.2: Penetration depth technical specification (from Anton Paar Nanoindentation tester NHT2 Technical Features Brochure).

	Fine range	Large range
Maximum indentation depth in μm	40	200
Depth resolution in nm	0.01	0.06
Noise floor (rms) in nm	0.3	
Maximum indenter travel range in μm	200	

Table 5.3: Indentation Test Parameters.

Parameter	Set Value
Acquisition Rate in Hz	60.0
Approach distance in nm	2500
Approach speed in nm/min	2500
Retract time in seconds	3
Stiffness threshold in $\mu N/\mu m$	500
Spring compliance in mm/N	0.95

5.5 Application of Nanoindentation Testing on Cortical Bone

The tests were carried out with a maximum indentation load of 0.5 mN and 2 mN upon the surface of the polished cortical bone in a square grid of 3x3, 5x5, 10x10, and 20x20 indents with a spacing of 10 μm. The tests were conducted on a completely flat surface on the specimen, in an area without large Haversian canals. 100 indentations were carried out on each of the specimens; examples of the residual indentation can be viewed in Figure 5.6.

The indentation loading rate was prescribed to be six times the indentation load per minute, and the prescribed holding time between loading and unloading was set at 5 seconds. The specified approach distance and speed are 2500 nm and 1500 nm/min respectively. The indenter retract speed is set to 2500 nm/min, and the retract time is set to 3 seconds. The instrument has been calibrated to have a stiffness threshold of 500 $\mu N/um$, and a spring compliance of 0.95 mm/N. These parameters are detailed in Table 5.3.

5.6 Analysis

This section discusses the nanoindentation analysis performed on longitudinally cut cortical bone specimens tested in the transverse direction during the research project.

Figure 5.6: Optical microscopy of indentations on surface of polished cortical bone.

(a) 20x magnification of an indent.

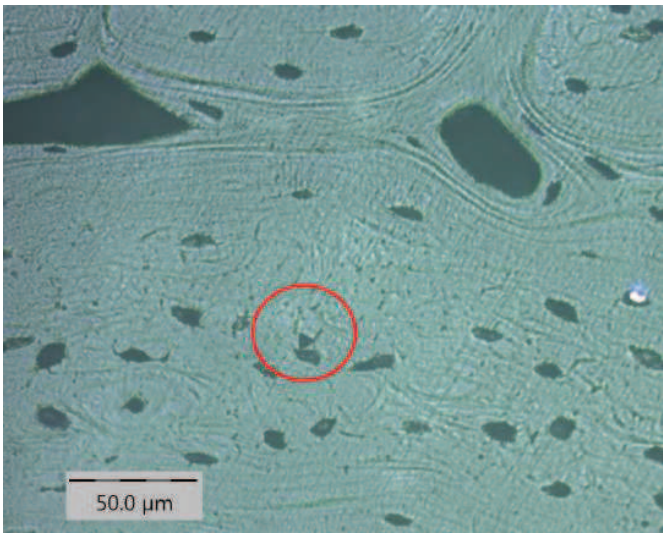

(b) 50x indent of an indent.

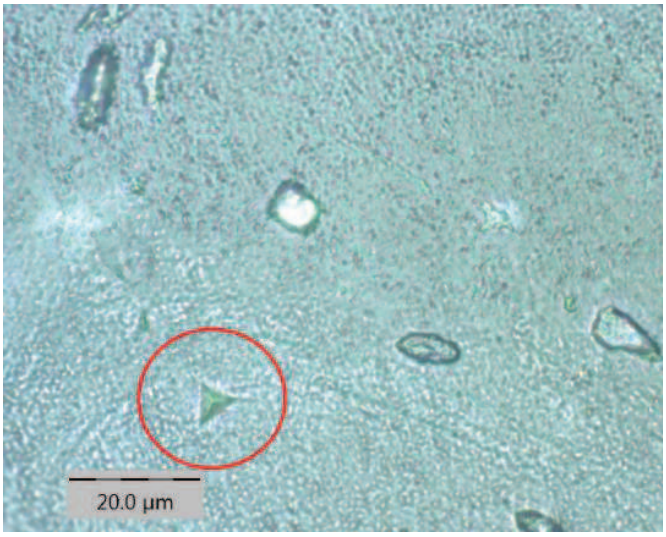

5.6.1 Load Penetration Depth

The test produces load-displacement curves, examples of which are displayed in Figure 5.7 and Figure 5.8 for porcine bone specimens, and Figure 5.9 and Figure 5.10 for bovine bone specimens. The penetration depth was around 1-1.7 μm for an indentation load of 0.5mN, and 3-4 μm for an indentation load of 2 mN, which confirms the aim of the research project to characterize cortical bone at the micro- and nano-scale. The hardness and elastic modulus of the specimen are calculated using the Oliver and Pharr method.

5.6.2 Porcine Specimens

For porcine bone specimens, the tests were carried out in square grids of varying sizes to provide a statistical basis for analysis through the accumulation of multiple data points within a small space on the specimen's polished surface. After the test is completed, all the results from the grid are compiled in a statistical deconvolution of the bulk data, which separates the different phases based on an initial guess for the number of constituent phases, and places each measurement within a specified phase. The theory of statistical deconvolution is applied to the results of the nanoindentation experiment as displayed in an example scatter plot in Figure 5.11, and shows the constituent phases within the tested area on the cortical bone. Example frequency plots, as displayed in Figure 5.12, show the distribution of the elastic modulus in Sub-Figure 5.12a, and the hardness in Sub-Figure 5.12b. The distribution of nanoindentation results is also displayed in Figure 5.13, where each indent is assigned an area and a modulus value as shown in Sub-Figure 5.13a and a phase as shown in Sub-Figure 5.13b. The contour maps are a spatial representation of the two phases as determined by the deconvoluted frequencies of their respective hardness and elas-

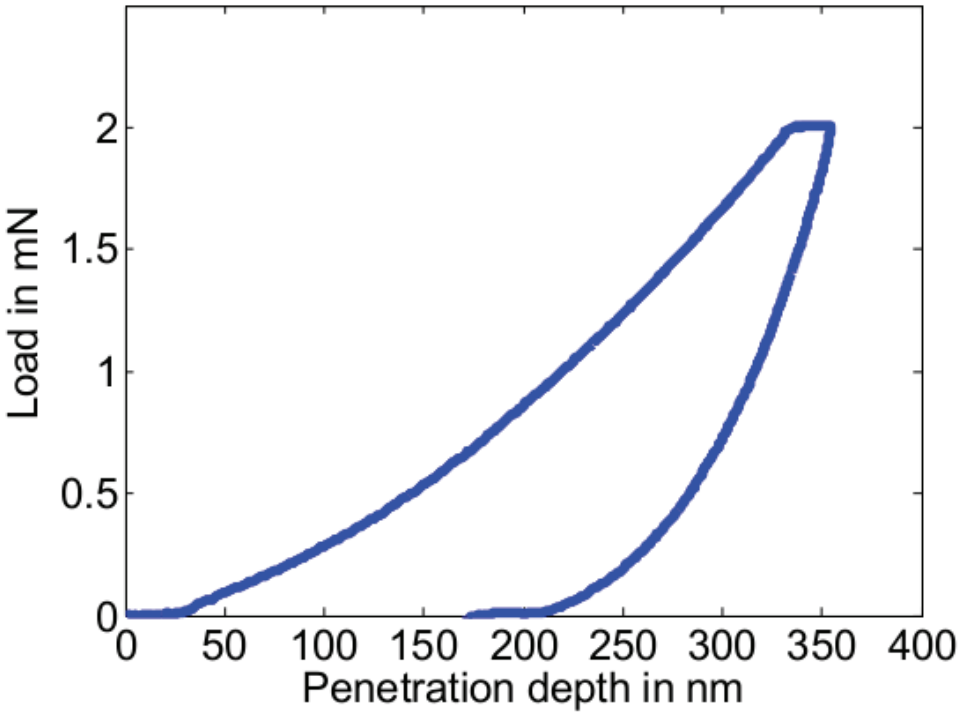

Figure 5.7: Example load-displacement curve for a 2-mN nanoindentation test on porcine bone.

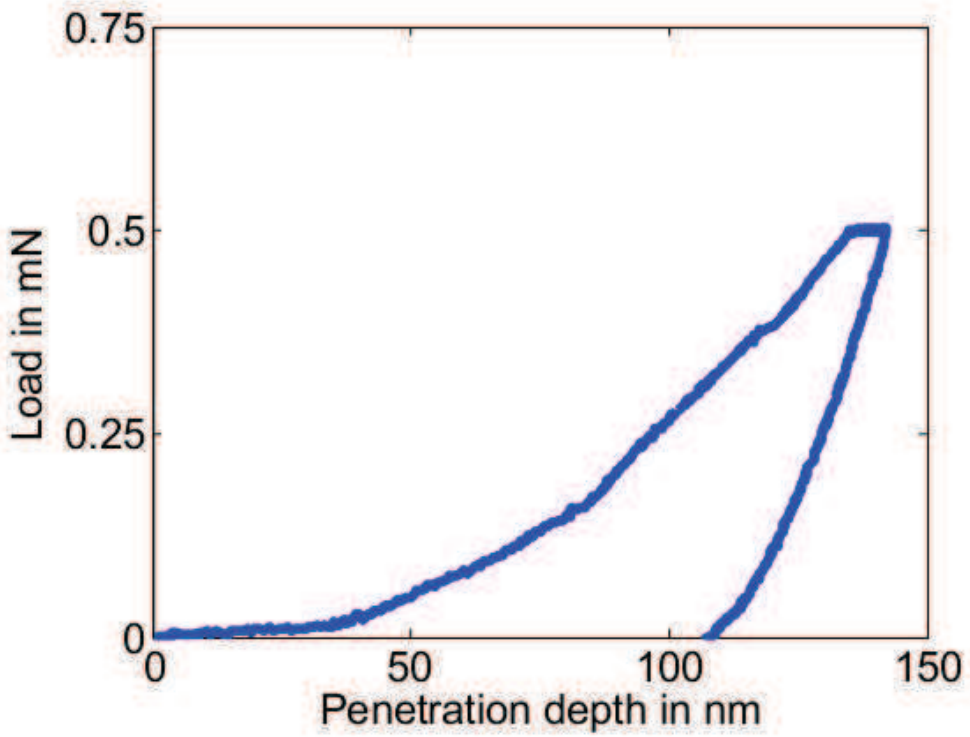

Figure 5.8: Example load-displacement curve for a 0.5-mN nanoindentation test on porcine bone.

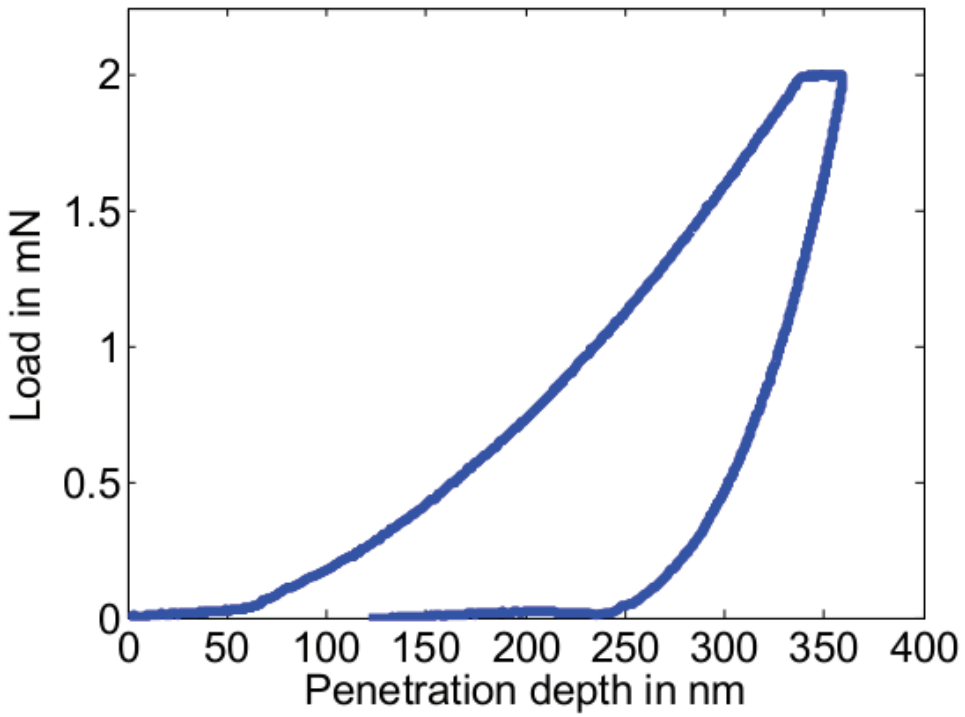

Figure 5.9: Example load-displacement curve for a 2-mN nanoindentation test on bovine bone.

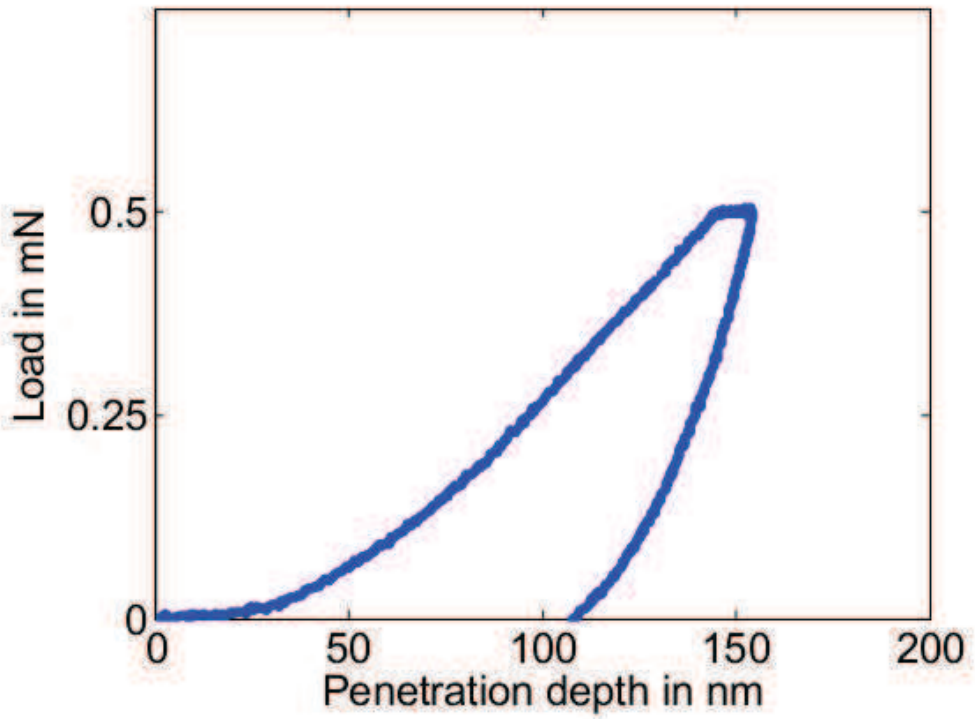

Figure 5.10: Example load-displacement curve for a 0.5-mN nanoindentation test on bovine bone.

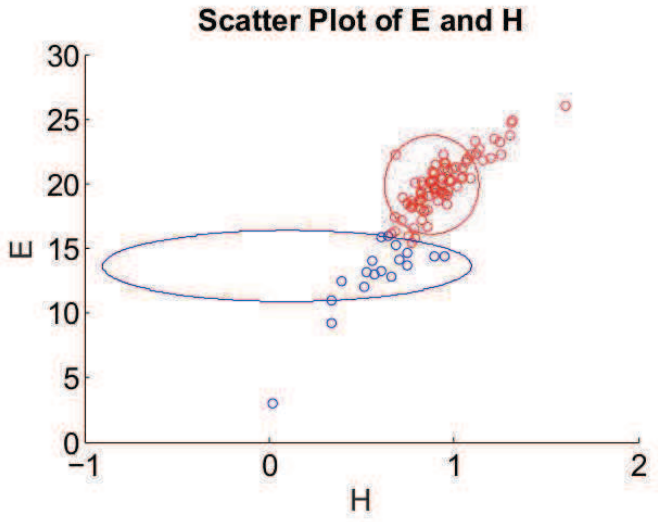

Figure 5.11: Example scatter plot of the hardness and elastic moduli results from a typical nanoindentation test. The elastic modulus, E, and the hardness, H, are in GPa.

tic moduli, as well as the interface between the two phases. Exanple contour maps are displayed in Figure 5.14. In Figure 5.14, Sub-Figure 5.14a features the modulus map, and Sub-figure 5.14b features the phase map. The modulus and phase maps are always identical, as the deconvoluted modulus results from the nanoindentation experiment directly impact the detected phases.

A large range of maximum loads were tried during the preliminary studies, and because two maximum indentation loads were utilized, more phases can be captured within the structure of the bone as the penetration depth is also varied. For the final investigation, 0.5 mN and 2 mN maximum indentation loads yielded results most consistent with the published literature, and are summarized in Table 5.4 and Table

Figure 5.12: Frequency plots for a 2 mN 10x10 grid nanoindentation test on porcine cortical bone.

(a) Example frequency plot for the elastic modulus.

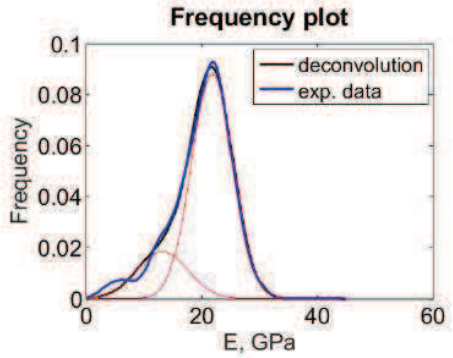

(b) Example frequency plot for the hardness.

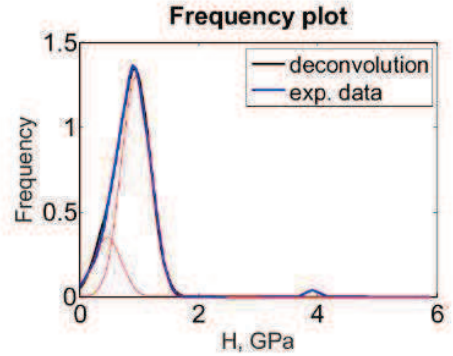

Figure 5.13: Modulus and phase grids of the tested region for a 2 mN 10x10 grid test on porcine cortical bone.

(a) Modulus grid.

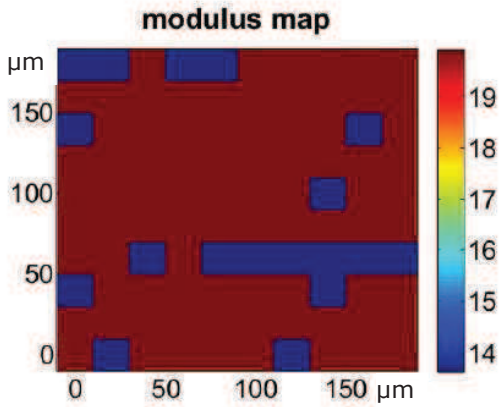

(b) Phase Grid.

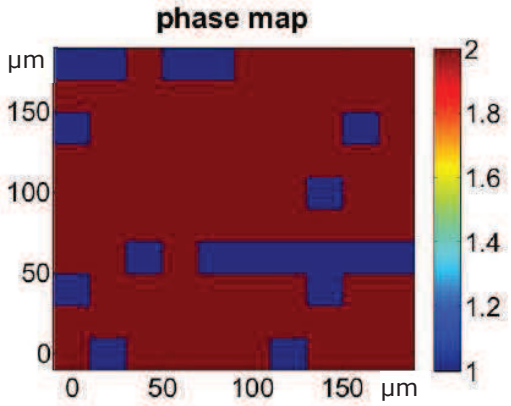

Figure 5.14: Modulus and phase maps of the tested region for a 2 mN 10x10 grid test on porcine cortical bone.

(a) Modulus map.

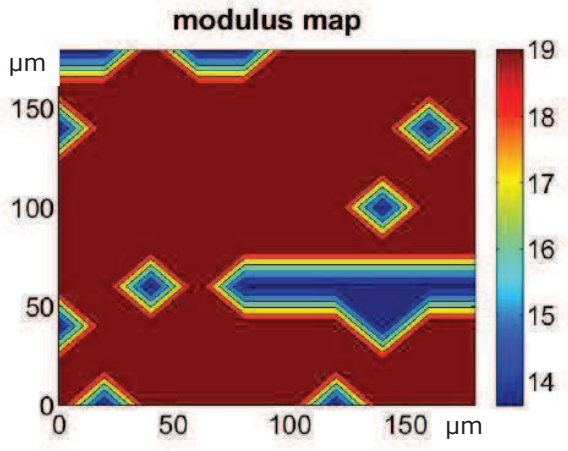

(b) Phase Map.

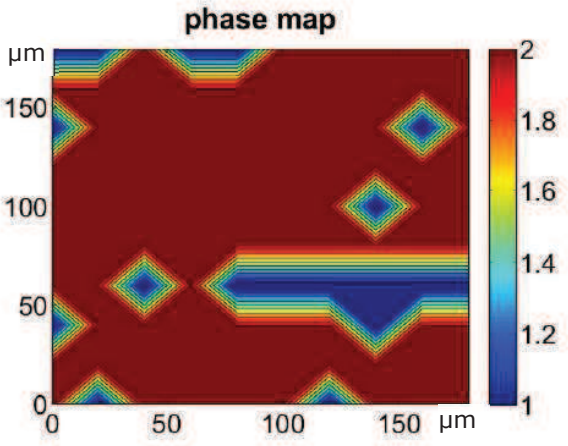

Table 5.4: Average results from statistical deconvolution of nanoindentation data for 0.5 mN loading rate.

Phase	Elastic Modulus (GPa)	Hardness (GPa)	Volume Fraction
1	12.90±4.38	0.62±0.36	0.24
2	22.04±3.47	0.92±0.37	0.76

Table 5.5: Average results from statistical deconvolution of nanoindentation data for 2 mN loading rate.

Phase	Elastic Modulus (GPa)	Hardness (GPa)	Volume Fraction
1	13.45±3.06	0.28±0.43	0.18
2	20.75±3.00	0.91±0.20	0.82

5.5. The statistical deconvolution provides results for the mean elastic modulus and hardness for each phase, as well as the volume fraction.

Refering to the literature review discussed in Section 2.4, phase one can be identified as the collagen fibril, and phase 2 can be identified as the osteonal tissue. Therefore, we can conclude that the presented procedure is accurate in determining the mechanical properties of bone on the micro- and nano- scale.

5.6.3 Bovine Specimens

Bovine specimens were indented in a 4 x 4 grid with a maximum load of 0.5 mN and 2 mN. Statistical deconvolution was not performed on the bovine specimens. The results from the nanoindentation were averaged and are displayed in Table 5.6. While the standard deviation is high for the elastic modulus, the mean is within the boundaries discovered in the literature as summarized in Section 2.4, confirming the accuracy of the presented protocol.

Table 5.6: Average results from nanoindentation of bovine specimens.

Mechanical Property	Mean and Standard Deviation(GPa)
Elastic Modulus	23.64±19.21
Hardness	0.80±0.48

5.7 Chapter Summary

In this chapter, nanoindentation is introduced as a crucial mechanical testing procedure for characterizing submicron mechanical properties in cortical bone. Contact mechanics forms the basis of nanoindentation as a hard tip of known mechanical properties is used to probe a material of unknown mechanical properties. Nanoindentation yields the elastic modulus and the hardness of the investigated material. With the presented protocol, two main phases are identified in the porcine cortical bone, with each phase having its own mean hardness and elastic modulus. The phases are then compared with the literature review summarized in Chapter 2. Bovine specimens were also indented, and the average values are reported and confirmed with the literature.

CHAPTER 6 SCRATCH TESTS

The toughness of bone is based upon the material's ability to resist fracture through several toughening mechanisms, ranging from crack bridging and deflection[164], and the development of a plastic zone at the crack tip[164]. The quality and resulting mechanical properties of bone are directly affected by a variety of factors which are relevant at different length scales. These factors include microstructural changes, microdamage formation, and the integrity and interaction of the constituents within bone [149]. Nanoindentation as a method of determining fracture toughness through the measurement of microcracks has been used to investigate bone at a submicron level, but is a limited technique in determining the fracture toughness due to the fact that microcracks have to already be present, and the methods used to measure the length of microcracks through image analysis may not be accurate or reproducible [149]. Therefore, a method is needed that can initiate cracks, and relates this crack initiation process with the material's ability to resist crack formation. Furthermore, this method should be reproducible, and fracture processes should be evident in the material after testing.

6.1 Introduction to Scratch Testing

Scratching is an action that has been used as a way of investigating material properties for a long time; people have always tested how hard a material is by subjecting it to a dragging force by another material. The process can be found in actions such as using a coin to scratch a lotto ticket and using a knife to scoop butter. Formal tests incorporating the scratching mechanism were introduced as early as 1824 with the advent of Moh's hardness scale, an empirical method for characterizing minerals by scratching the subject material with a harder material [4]. These scratch tests

are used today in several fields, ranging from geotechnical engineering and earth science to material science. In fact, scratch tests have been utilized in specialized applications such as in investigations of adhesion properties [149]. Scratch testing has also been used to determine mechanical properties of a variety of materials with different mechanical properties, including rocks [124, 132, 123, 11, 39], films and coatings [92, 25, 78, 74, 67, 68], polymers [69, 22, 34, 23, 24, 66], and biomechanical materials [4, 149, 105, 30].

6.2 Theory of Scratch Testing

The basic theory of scratch test is based upon the assumption and observation that fracture processes exist during the action of scratches. Scratch tests incorporate indentation into the specimen and cutting across the material to produce fracture processes; the resulting scratch groove is created by both plastic deformation of the bone specimen as well as tissue removal in the path of the scratch probe [149]. A generalized schematic of a scratch test is shown in Figure 6.1. Scratch tests and the resulting analysis must reconcile inherent fracture processes such as chipping with the shape and size of the material specimen, as well as the scratch probe's geometry and the resulting scratch depth in the specimen, as shown in Figure 6.2 [4].For fracture testing, the scratch is assumed to cause a crack within its path as it progresses during the experiment as shown in Figure 6.2.

The theory and model used in this study was first developed on a macroscopic scale to characterize the fracture processed in paraffin wax, a brittle material which was chosen for its linear elasticity and thermal stability [4]. The method was then applied on a microscopic level using specialized, high precision testing equipment. The resulting method of determining fracture properties through scratch testing is

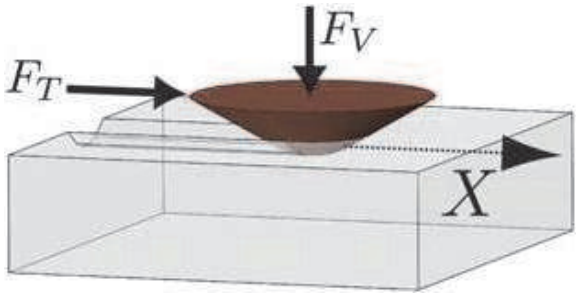

Figure 6.1: The basic model of a scratch test (from [3]).

Figure 6.2: Scratch test idealization (from [3]).

(a) Scratch probe seen from the side of the scratch probe.

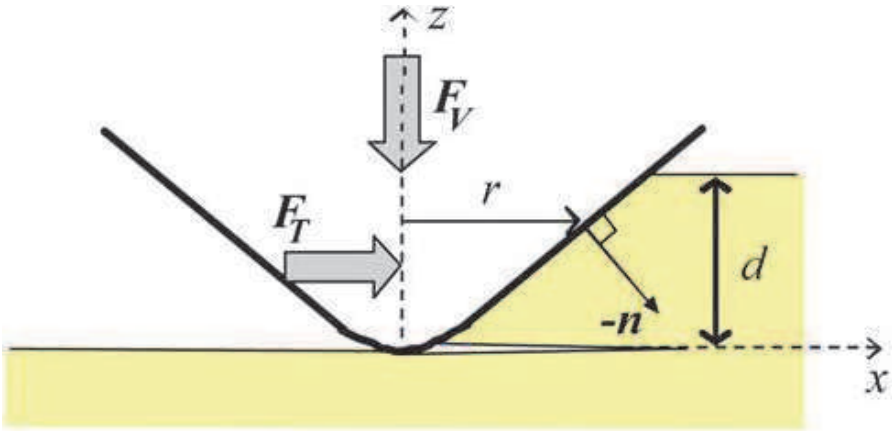

(b) Scratch probe seen from the front of the scratch probe.

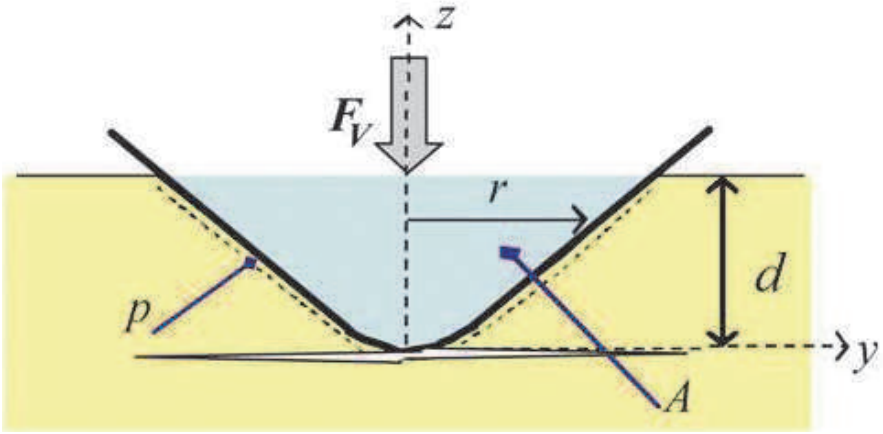

novel, reproducible, and requires smaller specimens which makes the technique almost nondestructive [3].

A typical scratch test relies on the recording of the resulting horizontal and vertical forces, F_T and F_V, as well as the penetration depth d. The underlying assumption is that the material is assumed to be homogenous and linearly elastic isotropic [3].

The model of a material undergoing scratch tests considers several factors based on the interface between the bone specimen and the scratch probe, represented by S. This interface is projected as an area onto the plane oriented perpendicularly to the x direction by the following relation:

$$A = \int_s -n_x dS$$

The model also incorporates the perimeter of the probe in contact with the material p, and the penetration depth d. The resulting uniaxial stress field ahead of the scratch probe can be represented by the following relation [3]:

$$\sigma_{xx} = -\frac{F_T}{A}$$

The model used to determine the fracture toughness from a scratch test analysis is based on linear elastic fracture mechanics, which determines the energy release rate of the interaction between the bone specimen and the scratch probe. This energy release rate is derived using a J-integral method, and the resultant stress intensity factor depends on the horizontal force F_T, the horizontal projected contact area A, and the perimeter p; the determination of the fracture toughness can be described by the following relation:

$$K_c = \frac{F_T}{[2pA]^{\frac{1}{2}}}$$

The stress intensity factor is completely dependent on the penetration depth in this model, as represented by the following function:

$$f = 2p(d)A(d)$$

The axi-symmetric geometry of the scratch indenter used in this investigation, which can be described as conical with a specified half-apex angle θ, rearranges the energy release rate representation into the following:

$$F_T \propto 2\frac{[\sin\theta]^{\frac{1}{2}}}{\cos\theta}K_c d^{\frac{3}{2}}$$

And the variable function dependent on the penetration depth becomes [3]:

$$f(d) = 4\frac{\sin\theta}{(\cos\theta)^2}d^3$$

6.3 Scratch Test Instrument

After the sample preparation procedure is completed, the specimen undergoes scratch testing using an MST Micro Scratch Tester platform designed by CSM Instruments, an Anton Paar division. The platform is displayed in displayed in Figure 6.3. Technical details of the MST module are detailed in Table 6.1. The MST platform is fitted with a Rockwell diamond indenter, which is modeled as a cone with a half-apex angle of $\theta = 60^o$ and a spherical tip radius of $R = 200\,\mu m$. The transition from the indenter's hemisphere to the cone occurs at $d/R = 0.13$, where d is the penetration depth. The software records the horizontal and vertical forces, F_V and F_T, as well as the penetration depth d. The software performs a prescan before proceeding with the scratch test, and a postscan afterwards. The prescan and postscan prescribe an

Figure 6.3: Micro Scratch Tester MST instrument (from Anton Paar Micro Scratch Tester MST Technical Features).

interaction between the probe and the specimen with a minute load of 0.03 N to measure the selected profile of the sample before and after the scratch occurs. The MST platform is equipped with a 4 position turret optical microscopy system that allows for panorama microscopy of the scratch groove.

6.4 Application of scratch testing

6.4.1 Scratch Probe Calibration

To determine the fracture toughness of the cortical bone specimens, the data must be evaluated with respect to the scratch probe shape function $2pA$ [5]. Therefore, a reference material is needed. For the presented research project, Lexan 9034, a standard polycarbonate, was selected. The fracture toughness of Lexan 9043 has been measured at 2.69 $MPa\sqrt{m}$ [5][65]. The material must be prepared by removing

Table 6.1: Micro-scratch technical specifications (from Anton Paar Micro Scratch Tester MST Technical Features).

	Fine range	Large range
Maximum load in N	10	30
Load Resolution in μN	10	30
Maximum penetration depth in μm	100	1000
Depth resolution in nm	0.05	0.5
Maximum friction load in N	10	30
Friction resolution in mN	0.1	1

any impurities on the surface and any excess moisture content through ultrasonic cleaning for 5 minutes in a 1% Alconox solution, ultrasonic cleaning for 5 minutes in deionized water, exposing all faces to a jet of deionized water, oven drying at 250^oF in clean glass jars for 24 hours, and cooling for 24 hours in a closed glass jar at room temperature [5]. The polycarbonate is then scratched and the scratch probe shape function is analyzed, as displayed in Figure 6.4. The coefficients of the scratch probe shape function correspond to the geometry of the probe; the first coefficient approximates the behavior of the cone, the second approximates a sphere, and the third a flat punch.

6.4.2 Scratch Testing Applied to Cortical Bone

The scratch tests were carried in the transverse direction across the osteon on longitudinally cut cortical bone specimens, as shown in the schematic in Figure 6.5. The scratch tests are conducted with a maximum load of 30 N, and a scratch speed of 4 mm/min. The loading rate was set at 60 N/min with a scratch length of 2 mm. The scratch tests were conducted on a completely flat surface of the specimen, in an area without large Haversian canals. The results are compiled in a graph displaying the applied normal force, the measured vertical force, and the penetration depth, as shown in Figure 6.6. The penetration depths ranged from 80 – 140 nm. Figure 6.6

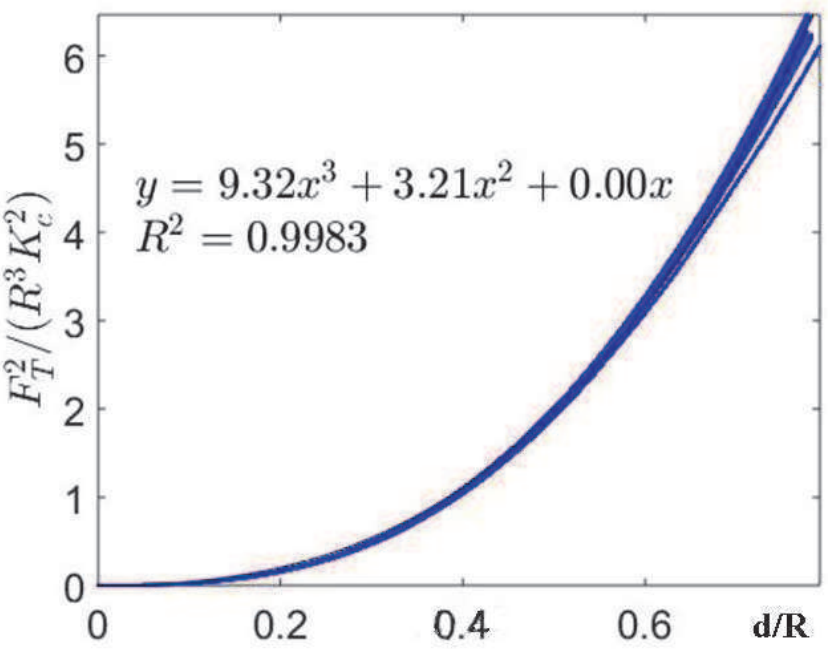

Figure 6.4: Representative Lexan 9043 calibration graph.

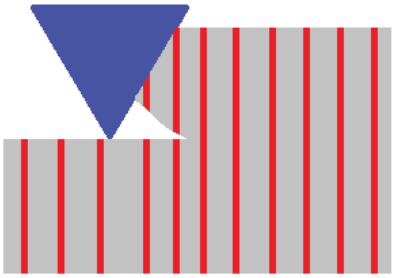

Figure 6.5: Schematic of a transverse scratch test on a longitudinally cut specimen. The red represents the osteons within the bone tissue, represented by the grey. The blue represents the scratch probe.

also displays the residual scratch groove as a result of the experiment.

6.5 Analysis of Scratch Test Results

6.5.1 Scaling of Scratch Force

The results from the scratch tests were scaled according to theory incorporating non-linear fracture mechanics and dimensional analysis [4, 3]. This scaling to determine the fracture toughness represented by the stress intensity factor was encoded in a MATLAB script which incorporated the data from the software included with the Anton Paar MST module. The scratch test scalings were calibrated using the scratch probe function as obtained from scratch tests conducted on Lexan 9034 polycarbonate, and examples are displayed in Figure 6.7.

The fracture scaling as shown in Figure 6.7 depicts the resulting processes during the scratch testing procedure. As the scratch test begins, the probe penetration depth is low, and the high initial K_c values are a result of the plastic dissipation. As the penetration depth increases, the probe begins cutting and removing material, which

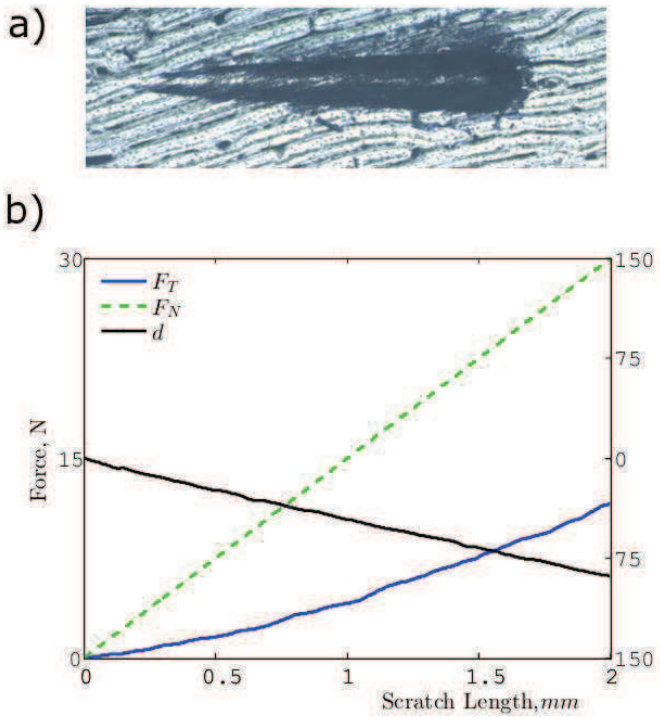

Figure 6.6: Example scratch test curve. a) optical microscopy of the scratch groove. b) information collected during the scratch test. F_T is the measured horizontal force, F_N is the applied normal force, and d is the penetration depth of the scratch probe into the bone tissue.

indicates fracture processes are taking place. Therefore, the K_c values plummet. The fracture toughness values as represented by the stress intensity factors are analyed in histograms for both porcine and bovine cortical bone specimens as displayed in Figure 6.8. The average determined through this method is consistently within the 2-5 $MPa\sqrt{m}$ proposed by the literature [163, 151, 150, 153, 128].

6.5.2 Roughness Measurements with Atomic Force Microscopy

Atomic force microscopy was utilized to measure the roughness of the sample topography to assess the quality of the polishing procedure. The microscopy was conducted at the Center for Microanalysis of Materials in the Frederick Seitz Materials Research Laboratory at the University of Illinois at Urbana-Champaign. An Asylum Research MFP-3D AFM instrument was utilized in the research; this instrument features sub-angstrom vertical resolution and piezo response imaging. A 40-μm by 40-μm area was scanned, and the average roughness, as measured by the root-mean-square of the height values, is 45.9 nm. The low roughness confirms the effectiveness of the final polishing procedure and validates the resulting micro- and nano-scale characterizations. The results of the AFM scans are displayed in Figure 6.9, with irregularities such as dust, bone tissue debris, or large Haversian canals masked.

6.5.3 Fracture Micro-mechanisms via SEM Observations

To confirm the existence of fracture processes in the bone, the specimens were imaged using a JEOL 6060LV General Purpose scanning electron microscope at the Center for the Frederick Seitz Materials Research Laboratory at the University of Illinois at Urbana-Champaign. The samples were not coated, and a piece of copper tape was used to connect the bone specimen to the aluminum disk to reduce charging and to promote a higher resolution in the micrographs. The micrographs were taken

Figure 6.7: Representative $K_c$value results from scratch test data. $K_c$values are in $MPa\sqrt{m}$, d is the penetration depth, $R = 200\,\mu m$is the probe tip radius, F_T is the horizontal force, and $2pA$ is the scratch probe shape function where A is the projected contact area and p is the perimeter.

(a) 2-mm scratch test on porcine cortical bone with a loading rate of 60 N/min.

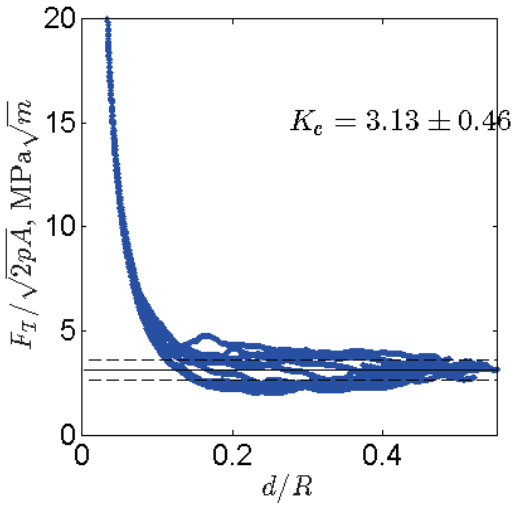

(b) 2-mm scratch test on bovine cortical bone with a loading rate of 60 N/min.

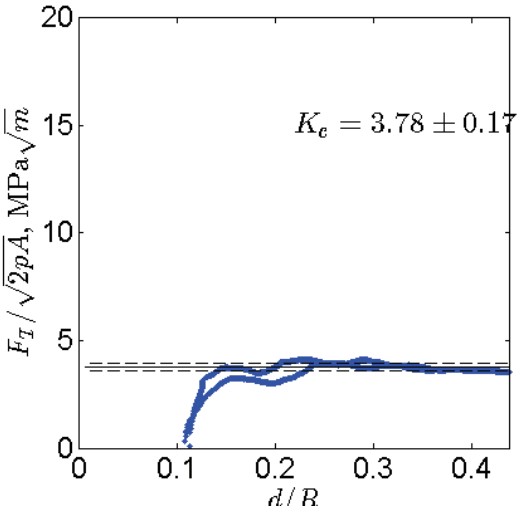

Figure 6.8: Histograms and average values for K_c.

(a) Histogram for porcine cortical bone specimens.

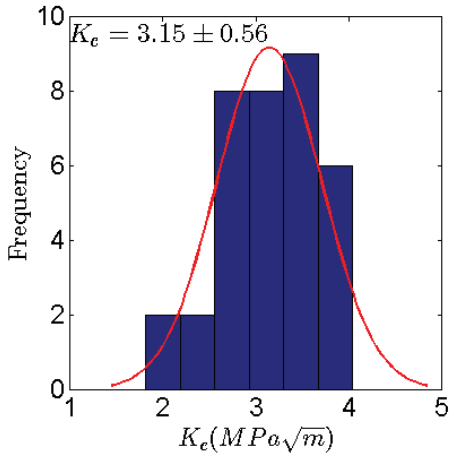

(b) Histogram for bovine cortical bone specimens.

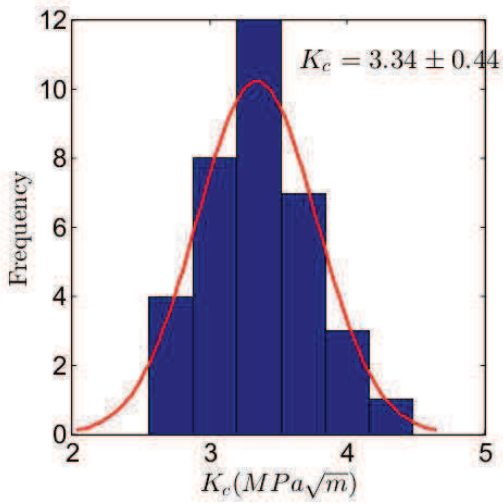

Figure 6.9: Atomic force microscopy scans of cortical bone.

(a) Atomic force microscopy scan 1.

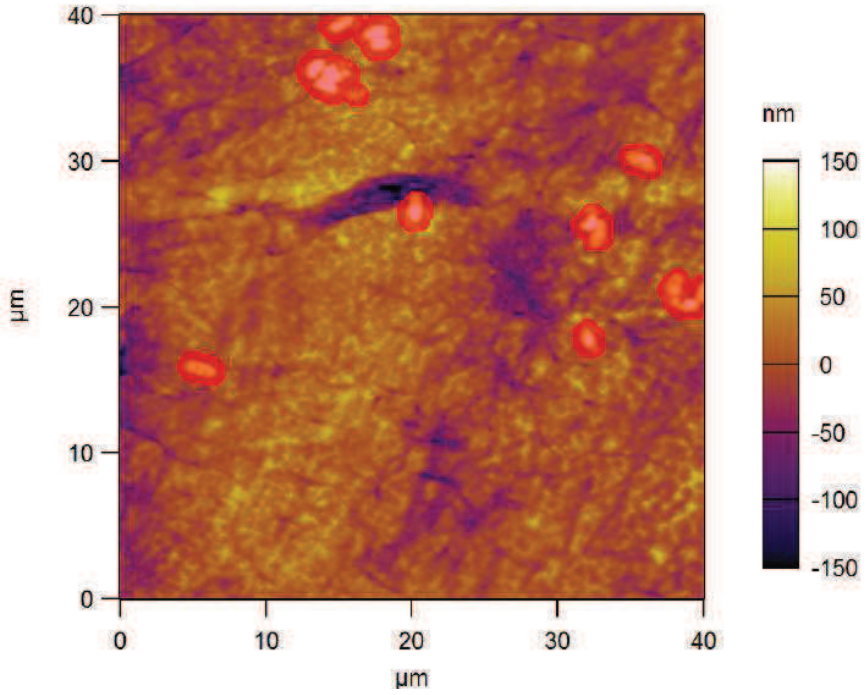

(b) Atomic force microscopy scan 2.

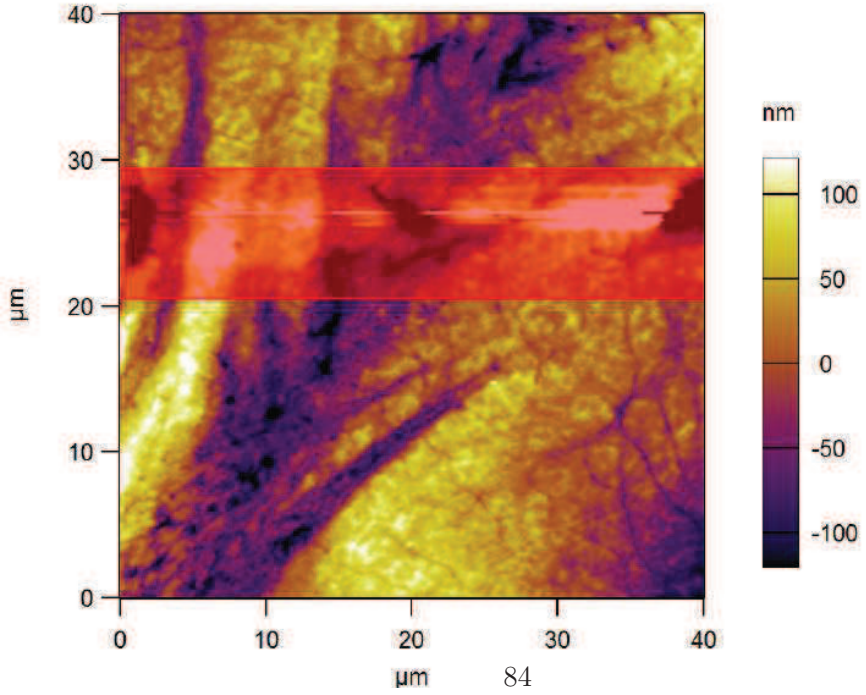

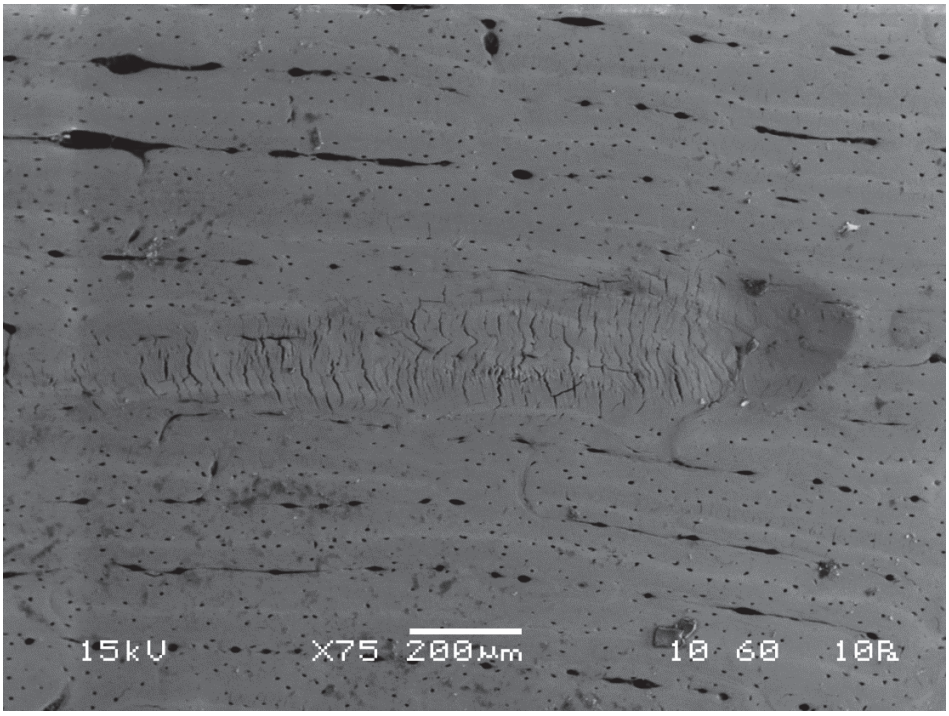

Figure 6.10: Scanning electron microscopy of 2-mm scratch on porcine cortical bone.

in a low-vacuum setting with an air pressure of 10 Pa. The SEM images featured crack bridging and deflection, as well as flaking. The appearance of these toughening mechanisms as shown in Figures 6.10, 6.11, and 6.12 proves that fracture was induced during the scratch test.

6.6 Chapter Summary

To determine the fracture toughness of bone in an almost nondestructive and high precision manner, the presented research focused on applying scratch tests to porcine and bovine bone tissue specimens. These specimens underwent progressive loading with a specified maximum force, loading rate, and scratch speed to create a scratch groove that could be analyzed visually for known toughening mechanisms. The data from the scratch tests were analyzed according to a MATLAB routine based upon theory

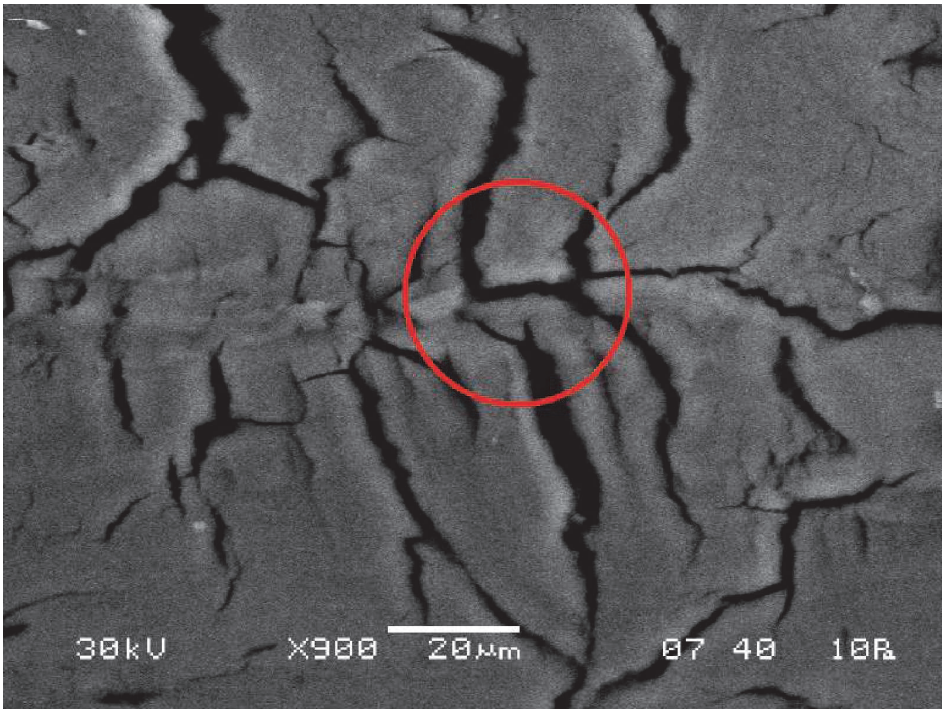

Figure 6.11: Scanning electron microscopy displaying crack deflection.

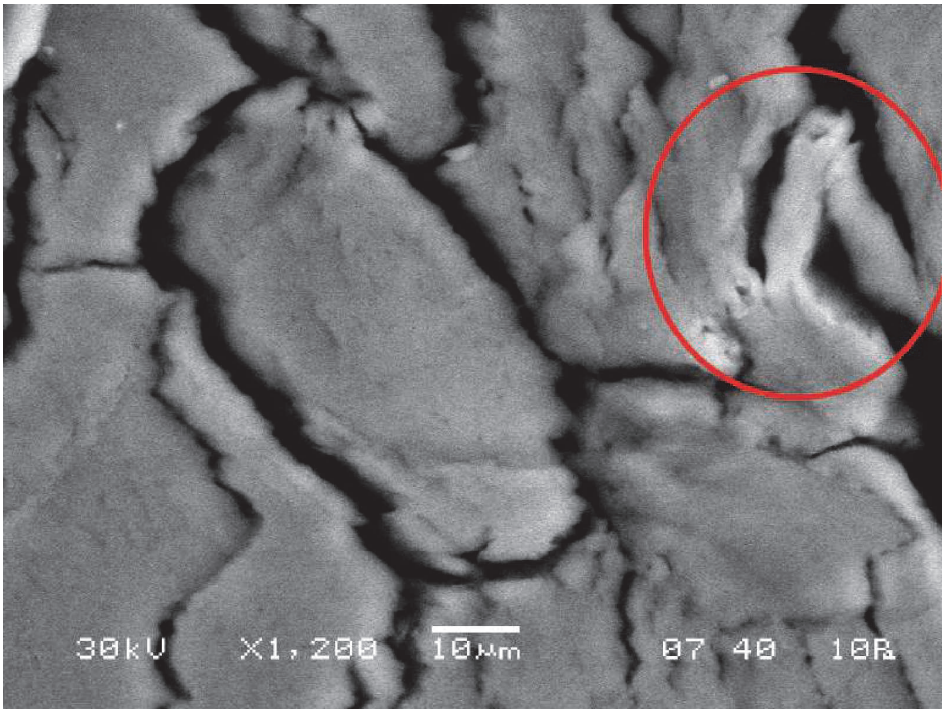

Figure 6.12: Scanning electron microscopy displaying crack bridging.

developed by Dr. Ange-Therese Akono. The routine produced a fracture toughness that fit into the ranges suggested by previous fracture toughness investigations in the literature.

CHAPTER 7 CONCLUSION AND PERSPECTIVES

The presented research applies small-scale testing to successfully characterize fracture processes within cortical bone. By developing a preparation procedure using specialized equipment in the Sustainability Under the Nanoscope Laboratory at the University of Illinois at Urbana-Champaign, consistent samples were created and tested using novel microscopic methods. Nanoindentation characterized the mechanical properties of bone by measuring the elastic modulus and the hardness, and microscratch tests characterized fracture processes in the bone by measuring the resultant fracture toughness as embodied in the stress intensity factor.

7.1 Summary of Main Findings

1. The application of nanoindentation on cortical bone was used to characterize areas of the bone surface through multiple tests in a grid pattern. The resulting hardnesses and elastic moduli yields two main phases, corresponding to the material comprising the osteonal tissue, and the material comprising the interstitial tissue.

2. The application of scratch testing to induce mixed mode fracture processes is a novel and valid method of characterizing fracture toughness through the stress intensity factor. The proof of the resulting fracture processes from the scratch test can be observed through scanning electron microscopy, which displays processes such as crack bridging and crack deflection. Furthermore, scratch tests can capture the inherent anisotropy within bone.

3. A model based in non-linear fracture mechanics is necessary to accurately characterize the fracture toughness of bone from the scratch test results.

7.2 Current Limitations

1. While the sample preparation procedures and the mechanical testing methods outlined in this thesis are novel in determining the mechanical properties of bone on a micro-structural scale, several properties of bone have yet to be determined at the nano-structural scale due to the lack of proper sample preparation and testing techniques available. In order to create a full picture of bone and its mechanical properties, further research is necessary for multiscale characterization. With this information, more accurate models of bones can be created to investigate exactly why bones break.

2. More experimentation is needed to discover if there is a size effect in bone, and if there is a critical size for the measurement of particular mechanical properties.

3. The influence of location on the mechanical properties of bone needs to be accounted for in future studies of micro-scale fracture characterization.

7.3 Conclusion

The procedures and results presented in this thesis were developed to display the feasibility of conducting novel micro-scale testing such as nanoindentation and scratch testing on a material as complex as bone tissue. The characterization of fracture processes through scratch tests is of particular interest because it aids in conserving specimens when testing, and displays the fracture processes as a result of mixed mode fracture in a way that bulk experiments cannot. The application of scratch testing yielded results that are in the range of those reported in previous experiments, therefore scratch testing is a valid experimental procedure for fracture characterization.

REFERENCES

[1] Joel W Ager, Ravi Kiran Nalla, Katherine L Breeden, and Robert O Ritchie. Deep-ultraviolet raman spectroscopy study of the effect of aging on human cortical bone. *Journal of Biomedical Optics*, 10(3):034012–0340128, 2005.

[2] JW Ager, G Balooch, and RO Ritchie. Fracture, aging, and disease in bone. *Journal of Materials Research*, 21(08):1878–1892, 2006.

[3] Ange-Therese Akono, Nicholas X Randall, and Franz-Josef Ulm. Experimental determination of the fracture toughness via microscratch tests: application to polymers, ceramics, and metals. *Journal of Materials Research*, 27(02):485–493, 2012.

[4] Ange-Therese Akono, PM Reis, and FJ Ulm. Scratching as a fracture process: From butter to steel. *Physical Review Letters*, 106(20):204–302, 2011.

[5] Ange-Therese Akono and Franz-Josef Ulm. An improved technique for characterizing the fracture toughness via scratch test experiments. *Wear*, 313(1):117–124, 2014.

[6] Yuehuei H An and Kylie L Martin. *Handbook of Histology Methods for Bone and Cartilage*. Springer, 2003.

[7] DF Bahr, DE Kramer, and WW Gerberich. Non-linear deformation mechanisms during nanoindentation. *Acta Materialia*, 46(10):3605–3617, 1998.

[8] Holly D Barth, Elizabeth A Zimmermann, Eric Schaible, Simon Y Tang, Tamara Alliston, and Robert O Ritchie. Characterization of the effects of x-ray irradiation on the hierarchical structure and mechanical properties of human cortical bone. *Biomaterials*, 32(34):8892–8904, 2011.

[9] JC Behiri and W Bonfield. Crack velocity dependence of longitudinal fracture in bone. *Journal of Materials Science*, 15(7):1841–1849, 1980.

[10] JC Behiri and W Bonfield. Orientation dependence of the fracture mechanics of cortical bone. *Journal of Biomechanics*, 22(8-9):863869–867872, 1989.

[11] Ulrik Beste, Axel Lundvall, and Staffan Jacobson. Micro-scratch evaluation of rock types—a means to comprehend rock drill wear. *Tribology International*, 37(2):203–210, 2004.

[12] Rahul Bhowmik, Kalpana S Katti, and Dinesh R Katti. Mechanics of molecular collagen is influenced by hydroxyapatite in natural bone. *Journal of Materials Science*, 42(21):8795–8803, 2007.

[13] B Bhushan. Handbook of micro/nanotribology, 1995. *CRC, Bota Raton*, 1998.

[14] MS Bobji and SK Biswas. Estimation of hardness by nanoindentation of rough surfaces. *Journal of Materials Research*, 13(11):3227–3233, 1998.

[15] A Bolshakov, WC Oliver, and GM Pharr. An explanation for the shape of nanoindentation unloading curves based on finite element simulation. In *MRS Proceedings*, volume 356, page 675. Cambridge Univ Press, 1994.

[16] LC Bonar, AH Roufosse, WK Sabine, MD Grynpas, and MJ Glimcher. X-ray diffraction studies of the crystallinity of bone mineral in newly synthesized and density fractionated bone. *Calcified Tissue International*, 35(1):202–209, 1983.

[17] W Bonfield. Advances in the fracture mechanics of cortical bone. *Journal of Biomechanics*, 20(11-12):1071–1081, 1987.

[18] W Bonfield and PK Datta. Fracture toughness of compact bone. *Journal of Biomechanics*, 9(3):131–134, 1976.

[19] W Bonfield, MD Grynpas, and RJ Young. Crack velocity and the fracture of bone. *Journal of Biomechanics*, 11(10-12):473–479, 1978.

[20] Joseph Boussinesq. *Application des potentiels à l'étude de l'équilibre et du mouvement des solides élastiques: principalement au calcul des déformations et des pressions que produisent, dans ces solides, des efforts quelconques exercés sur une petite partie de leur surface ou de leur intérieur: mémoire suivi de notes étendues sur divers points de physique, mathematique et d'analyse*, volume 4. Gauthier-Villars, 1885.

[21] BJ Briscoe, L Fiori, and E Pelillo. Nano-indentation of polymeric surfaces. *Journal of Physics D: Applied Physics*, 31(19):2395, 1998.

[22] RL Browning, G-T Lim, A Moyse, H-J Sue, H Chen, and JD Earls. Quantitative evaluation of scratch resistance of polymeric coatings based on a standardized progressive load scratch test. *Surface and Coatings Technology*, 201(6):2970–2976, 2006.

[23] Jean-Luc Bucaille, Eric Felder, and Gilles Hochstetter. Experimental and three-dimensional finite element study of scratch test of polymers at large deformations. *Journal of Tribology*, 126(2):372–379, 2004.

[24] JL Bucaille, E Felder, and G Hochstetter. Mechanical analysis of the scratch test on elastic and perfectly plastic materials with the three-dimensional finite element modeling. *Wear*, 249(5):422–432, 2001.

[25] SJ Bull. Failure mode maps in the thin film scratch adhesion test. *Tribology International*, 30(7):491–498, 1997.

[26] SJ Bull and EG Berasetegui. An overview of the potential of quantitative coating adhesion measurement by scratch testing. *Tribology International*, 39(2):99–114, 2006.

[27] Russel Burge, Bess Dawson-Hughes, Daniel H Solomon, John B Wong, Alison King, and Anna Tosteson. Incidence and economic burden of osteoporosis-related fractures in the united states, 2005–2025. *Journal of Bone and Mineral Research*, 22(3):465–475, 2007.

[28] David B Burr, Charles H Turner, Pratap Naick, Mark R Forwood, Walter Ambrosius, M Sayeed Hasan, and Ramana Pidaparti. Does microdamage accumulation affect the mechanical properties of bone? *Journal of Biomechanics*, 31(4):337–345, 1998.

[29] Albert H Burstein, Donald T Reilly, and Marc Martens. Aging of bone tissue: mechanical properties. *J Bone Joint Surg Am*, 58(1):82–86, 1976.

[30] Frank Butz, Hideki Aita, Kazuo Takeuchi, and Takahiro Ogawa. Enhanced mineralized tissue adhesion to titanium over polystyrene assessed by the nano-scratch test. *Journal of Biomedical Materials Research Part A*, 74(2):164–170, 2005.

[31] Davide Carnelli, Riccardo Lucchini, Matteo Ponzoni, Roberto Contro, and Pasquale Vena. Nanoindentation testing and finite element simulations of cortical bone allowing for anisotropic elastic and inelastic mechanical response. *Journal of Biomechanics*, 44(10):1852–1858, 2011.

[32] Dennis R Carter and Wilson C Hayes. Compact bone fatigue damage: a microscopic examination. *Clinical Orthopaedics and Related Research*, 127:265–274, 1977.

[33] Michele Colloca, Romane Blanchard, Christian Hellmich, Keita Ito, and Bert van Rietbergen. A multiscale analytical approach for bone remodeling simulations: linking scales from collagen to trabeculae. *Bone*, 64:303–313, 2014.

[34] R Consiglio, NX Randall, B Bellaton, and J Von Stebut. The nano-scratch tester (nst) as a new tool for assessing the strength of ultrathin hard coatings and the mar resistance of polymer films. *Thin Solid Films*, 332(1):151–156, 1998.

[35] Georgios Constantinides and Franz-Josef Ulm. The nanogranular nature of c–s–h. *Journal of the Mechanics and Physics of Solids*, 55(1):64–90, 2007.

[36] DML Cooper, AL Turinsky, CW Sensen, and B Hallgrimsson. Quantitative 3d analysis of the canal network in cortical bone by micro-computed tomography. *The Anatomical Record Part B: The New Anatomist*, 274(1):169–179, 2003.

[37] JD Currey. Effects of differences in mineralization on the mechanical properties of bone. *Philosophical Transactions of the Royal Society B: Biological Sciences*, 304(1121):509–518, 1984.

[38] John D Currey. The structure and mechanics of bone. *Journal of Materials Science*, 47(1):41–54, 2012.

[39] Fabrice Dagrain, Edmond Poyol, and Thomas Richard. Strength logging of geomaterials from scratch tests. *Proceedings of the Rock Engineering Theory and Practice*, pages 635–640, 2004.

[40] Wilfrid T Dempster and Richard T Liddicoat. Compact bone as a non-isotropic material. *American Journal of Anatomy*, 91(3):331–362, 1952.

[41] Vladislav Domnich, Yury Gogotsi, and Sergey Dub. Effect of phase transformations on the shape of the unloading curve in the nanoindentation of silicon. *Applied Physics Letters*, 76(16):2214–2216, 2000.

[42] M Elices, GV Guinea, J Gomez, and J Planas. The cohesive zone model: advantages, limitations and challenges. *Engineering Fracture Mechanics*, 69(2):137–163, 2002.

[43] Horacio D Espinosa, Jee E Rim, Francois Barthelat, and Markus J Buehler. Merger of structure and material in nacre and bone–perspectives on de novo biomimetic materials. *Progress in Materials Science*, 54(8):1059–1100, 2009.

[44] Z Fan, JG Swadener, JY Rho, ME Roy, and GM Pharr. Anisotropic properties of human tibial cortical bone as measured by nanoindentation. *Journal of Orthopaedic Research*, 20(4):806–810, 2002.

[45] Liang Feng, Michael Chittenden, Jeffrey Schirer, Michelle Dickinson, and Iwona Jasiuk. Mechanical properties of porcine femoral cortical bone measured by nanoindentation. *Journal of Biomechanics*, 45(10):1775–1782, 2012.

[46] Liang Feng and Iwona Jasiuk. Multi-scale characterization of swine femoral cortical bone. *Journal of Biomechanics*, 44(2):313–320, 2011.

[47] AC Fischer-Cripps. A review of analysis methods for sub-micron indentation testing. *Vacuum*, 58(4):569–585, 2000.

[48] ER Fitzgerald. Dynamic mechanical measurements during the life to death transition in animal tissues. *Biorheology*, 12(6):397–408, 1975.

[49] P Fratzl, HS Gupta, EP Paschalis, and P Roschger. Structure and mechanical quality of the collagen–mineral nano-composite in bone. *Journal of Materials Chemistry*, 14(14):2115–2123, 2004.

[50] Peter Fratzl. Bone fracture: When the cracks begin to show. *Nature Materials*, 7(8):610–612, 2008.

[51] Andreas Fritsch and Christian Hellmich. 'universal'microstructural patterns in cortical and trabecular, extracellular and extravascular bone materials: micromechanics-based prediction of anisotropic elasticity. *Journal of Theoretical Biology*, 244(4):597–620, 2007.

[52] Andreas Fritsch, Christian Hellmich, and Luc Dormieux. Ductile sliding between mineral crystals followed by rupture of collagen crosslinks: experimentally supported micromechanical explanation of bone strength. *Journal of Theoretical Biology*, 260(2):230–252, 2009.

[53] Lev Aleksandrovich Galin, H Moss, and Ian Naismith Sneddon. Contact problems in the theory of elasticity. Technical report, DTIC Document, 1961.

[54] Jianghong Gong, Hezhuo Miao, and Zhijian Peng. On the contact area for nanoindentation tests with berkovich indenter: case study on soda-lime glass. *Materials Letters*, 58(7):1349–1353, 2004.

[55] A Gouldstone, H-J Koh, K-Y Zeng, AE Giannakopoulos, and S Suresh. Discrete and continuous deformation during nanoindentation of thin films. *Acta Materialia*, 48(9):2277–2295, 2000.

[56] Elham Hamed, Yikhan Lee, and Iwona Jasiuk. Multiscale modeling of elastic properties of cortical bone. *Acta Mechanica*, 213(1-2):131–154, 2010.

[57] Fei Hang and Asa H Barber. Nano-mechanical properties of individual mineralized collagen fibrils from bone tissue. *Journal of The Royal Society Interface*, 8(57):500–505, 2011.

[58] Christian Hellmich. Microelasticity of bone. In *Applied Micromechanics of Porous Materials*, pages 289–331. Springer, 2005.

[59] Christian Hellmich, Jean-Francois Barthélémy, and Luc Dormieux. Mineral–collagen interactions in elasticity of bone ultrastructure–a continuum micromechanics approach. *European Journal of Mechanics-A/Solids*, 23(5):783–810, 2004.

[60] Christian Hellmich and F-J Ulm. Average hydroxyapatite concentration is uniform in the extracollagenous ultrastructure of mineralized tissues: evidence at the 1–10-μm scale. *Biomechanics and Modeling in Mechanobiology*, 2(1):21–36, 2003.

[61] Christian Hellmich and Franz-Josef Ulm. Micromechanical model for ultrastructural stiffness of mineralized tissues. *Journal of Engineering Mechanics*, 128(8):898–908, 2002.

[62] S Hengsberger, A Kulik, and Ph Zysset. A combined atomic force microscopy and nanoindentation technique to investigate the elastic properties of bone structural units. *Eur Cell Mater*, 1:12–17, 2001.

[63] EG Herbert, GM Pharr, WC Oliver, BN Lucas, and JL Hay. On the measurement of stress–strain curves by spherical indentation. *Thin Solid Films*, 398:331–335, 2001.

[64] Heinrich Hertz. *The principles of mechanics presented in a new form*. Courier Corporation, 1899.

[65] RW Hertzberg, MD Skibo, and JA Manson. Fatigue crack propagation in polyacetal. *Journal of Materials Science*, 13(5):1038–1044, 1978.

[66] Alma Hodzic, Jang Kyo Kim, and ZH Stachurski. Nano-indentation and nano-scratch of polymer/glass interfaces. ii: model of interphases in water aged composite materials. *Polymer*, 42(13):5701–5710, 2001.

[67] Liye Huang, Jian Lu, and Kewei Xu. Elasto-plastic deformation and fracture mechanism of a diamond-like carbon film deposited on a ti–6al–4v substrate in nano-scratch test. *Thin Solid Films*, 466(1):175–182, 2004.

[68] TR Hull, JS Colligon, and AE Hill. Measurement of thin film adhesion. *Vacuum*, 37(3):327–330, 1987.

[69] Vincent D Jardret and Warren C Oliver. Viscoelastic behavior of polymer films during scratch test: A quantitative analysis. In *MRS Proceedings*, volume 594, page 251. Cambridge Univ Press, 1999.

[70] S Jayaraman, GT Hahn, WC Oliver, CA Rubin, and PC Bastias. Determination of monotonic stress-strain curve of hard materials from ultra-low-load indentation tests. *International Journal of Solids and Structures*, 35(5):365–381, 1998.

[71] Huaidong Jiang, Damien Ramunno-Johnson, Changyong Song, Bagrat Amirbekian, Yoshiki Kohmura, Yoshinori Nishino, Yukio Takahashi, Tetsuya Ishikawa, and Jianwei Miao. Nanoscale imaging of mineral crystals inside bio-

logical composite materials using x-ray diffraction microscopy. *Physical Review Letters*, 100(3):038103, 2008.

[72] Olof Johnell and JA Kanis. An estimate of the worldwide prevalence and disability associated with osteoporotic fractures. *Osteoporosis International*, 17(12):1726–1733, 2006.

[73] JA Kanis, World Health Organization Scientific Group, et al. Who technical report. *University of Sheffield, UK*, 66, 2007.

[74] MM Karnowsky and WB Estill. Scratch test for measuring adherence of thin films to oxide substrates. *Review of Scientific Instruments*, 35(10):1324–1326, 1964.

[75] J-J Kim, Y Choi, S Suresh, and AS Argon. Nanocrystallization during nanoindentation of a bulk amorphous metal alloy at room temperature. *Science*, 295(5555):654–657, 2002.

[76] Kurt J Koester, JW Ager, and RO Ritchie. The true toughness of human cortical bone measured with realistically short cracks. *Nature Materials*, 7(8):672–677, 2008.

[77] Dusan Krajcinovic, Jordan Trafimow, and Dragoslav Sumarac. Simple constitutive model for a cortical bone. *Journal of Biomechanics*, 20(8):779–784, 1987.

[78] Michael T Laugier. An energy approach to the adhesion of coatings using the scratch test. *Thin Solid Films*, 117(4):243–249, 1984.

[79] Maximilien E Launey, P-Y Chen, Joanna McKittrick, and Robert O Ritchie. Mechanistic aspects of the fracture toughness of elk antler bone. *Acta Biomaterialia*, 6(4):1505–1514, 2010.

[80] Dong Li, Yip-Wah Chung, Ming-Show Wong, and William D Sproul. Nanoindentation studies of ultrahigh strength carbon nitride thin films. *Journal of Applied Physics*, 74(1):219–223, 1993.

[81] Xiaodong Li and Bharat Bhushan. A review of nanoindentation continuous stiffness measurement technique and its applications. *Materials Characterization*, 48(1):11–36, 2002.

[82] Frank Linde and Hans Christian Florian Sørensen. The effect of different storage methods on the mechanical properties of trabecular bone. *Journal of Biomechanics*, 26(10):1249–1252, 1993.

[83] H Lu, B Wang, J Ma, G Huang, and H Viswanathan. Measurement of creep compliance of solid polymers by nanoindentation. *Mechanics of Time-Dependent Materials*, 7(3-4):189–207, 2003.

[84] BN Lucas, WC Oliver, GM Pharr, and JL Loubet. Time dependent deformation during indentation testing. In *MRS Proceedings*, volume 436, page 233. Cambridge Univ Press, 1996.

[85] CL Malik, Susan M Stover, RB Martin, and JC Gibeling. Equine cortical bone exhibits rising r-curve fracture mechanics. *Journal of Biomechanics*, 36(2):191–198, 2003.

[86] R Bruce Martin. Determinants of the mechanical properties of bones. *Journal of Biomechanics*, 24:79–88, 1991.

[87] R Bruce Martin, David B Burr, and Neil A Sharkey. *Skeletal Tissue Mechanics*, volume 190. Springer, 1998.

[88] John W Melvin. Fracture mechanics of bone. *Journal of Biomechanical Engineering*, 115(4B):549–554, 1993.

[89] JW Melvin and FG Evans. Crack propagation in bone. In *ASME Biomechanics Symposium, New York*, 1973.

[90] Mahalia Miller, Christopher Bobko, Matthieu Vandamme, and Franz-Josef Ulm. Surface roughness criteria for cement paste nanoindentation. *Cement and Concrete Research*, 38(4):467–476, 2008.

[91] Leon Mishnaevsky Jr. Micromechanics of hierarchical materials: a brief overview. *Rev. Adv. Mater. Sci*, 30:60–72, 2012.

[92] Kashmiri Lal Mittal. *Adhesion Measurement of Films and Coatings*, volume 640. VSP, 1995.

[93] S Mohsin, FJ O'Brien, and TC Lee. Osteonal crack barriers in ovine compact bone. *Journal of Anatomy*, 208(1):81–89, 2006.

[94] LP Mullins, MS Bruzzi, and PE McHugh. Measurement of the microstructural fracture toughness of cortical bone using indentation fracture. *Journal of Biomechanics*, 40(14):3285–3288, 2007.

[95] Etienne Munch, Maximimilan E Launey, Daan H Alsem, Eduardo Saiz, Antoni P Tomsia, and Robert O Ritchie. Tough, bio-inspired hybrid materials. *Science*, 322(5907):1516–1520, 2008.

[96] R Kinney Nalla, John H Kinney, and Robert O Ritchie. Mechanistic fracture criteria for the failure of human cortical bone. *Nature Materials*, 2(3):164–168, 2003.

[97] R Kruzic Nalla, Jamie J Kruzic, John H Kinney, and Robert O Ritchie. Mechanistic aspects of fracture and r-curve behavior in human cortical bone. *Biomaterials*, 26(2):217–231, 2005.

[98] Ravi K Nalla, Jamie J Kruzic, and Robert O Ritchie. On the origin of the toughness of mineralized tissue: microcracking or crack bridging? *Bone*, 34(5):790–798, 2004.

[99] RK Nalla, JS Stölken, JH Kinney, and RO Ritchie. Fracture in human cortical bone: local fracture criteria and toughening mechanisms. *Journal of Biomechanics*, 38(7):1517–1525, 2005.

[100] Svetoslav Nikolov and Dierk Raabe. Hierarchical modeling of the elastic properties of bone at submicron scales: the role of extrafibrillar mineralization. *Biophysical Journal*, 94(11):4220–4232, 2008.

[101] William D Nix. Elastic and plastic properties of thin films on substrates: nanoindentation techniques. *Materials Science and Engineering: A*, 234:37–44, 1997.

[102] Timothy L Norman, D Vashishth, and David B Burr. Effect of groove on bone fracture toughness. *Journal of Biomechanics*, 25(12):1489–1492, 1992.

[103] TL Norman, D Vashishth, and David B Burr. Mode i fracture toughness of human bone. In *Publ by ASME*, 1991.

[104] Jeffry S Nyman, Michael Reyes, and Xiaodu Wang. Effect of ultrastructural changes on the toughness of bone. *Micron*, 36(7):566–582, 2005.

[105] Fergal J O'Brien, David Taylor, and T Clive Lee. An improved labelling technique for monitoring microcrack growth in compact bone. *Journal of Biomechanics*, 35(4):523–526, 2002.

[106] Fergal J O'Brien, David Taylor, and T Clive Lee. Microcrack accumulation at different intervals during fatigue testing of compact bone. *Journal of Biomechanics*, 36(7):973–980, 2003.

[107] Fergal J O'Brien, David Taylor, and T Clive Lee. The effect of bone microstructure on the initiation and growth of microcracks. *Journal of Orthopaedic Research*, 23(2):475–480, 2005.

[108] GM Odegard, TS Gates, and HM Herring. Characterization of viscoelastic properties of polymeric materials through nanoindentation. *Experimental Mechanics*, 45(2):130–136, 2005.

[109] Jim Oeppen and James W Vaupel. Broken limits to life expectancy. *Science*, 296(5570):1029–1031, 2002.

[110] Warren C Oliver and George M Pharr. Measurement of hardness and elastic modulus by instrumented indentation: Advances in understanding and refinements to methodology. *Journal of Materials Research*, 19(01):3–20, 2004.

[111] Warren Carl Oliver and George Mathews Pharr. An improved technique for determining hardness and elastic modulus using load and displacement sensing indentation experiments. *Journal of Materials Research*, 7(06):1564–1583, 1992.

[112] Herwig Peterlik, Paul Roschger, Klaus Klaushofer, and Peter Fratzl. From brittle to ductile fracture of bone. *Nature Materials*, 5(1):52–55, 2006.

[113] GM Pharr. Measurement of mechanical properties by ultra-low load indentation. *Materials Science and Engineering: A*, 253(1):151–159, 1998.

[114] GM Pharr and WC Oliver. Measurement of thin film mechanical properties using nanoindentation. *MRS Bulletin*, 17(07):28–33, 1992.

[115] GM Pharr, WC Oliver, and FR Brotzen. On the generality of the relationship among contact stiffness, contact area, and elastic modulus during indentation. *Journal of Materials Research*, 7(03):613–617, 1992.

[116] Shashindra M Pradhan, Kalpana S Katti, and Dinesh R Katti. Structural hierarchy controls deformation behavior of collagen. *Biomacromolecules*, 13(8):2562–2569, 2012.

[117] Donald T Reilly and Albert H Burstein. The elastic and ultimate properties of compact bone tissue. *Journal of Biomechanics*, 8(6):393IN9397–396IN11405, 1975.

[118] Jae Young Rho, Richard B Ashman, and Charles H Turner. Young's modulus of trabecular and cortical bone material: ultrasonic and microtensile measurements. *Journal of Biomechanics*, 26(2):111–119, 1993.

[119] Jae-Young Rho, Liisa Kuhn-Spearing, and Peter Zioupos. Mechanical properties and the hierarchical structure of bone. *Medical Engineering & Physics*, 20(2):92–102, 1998.

[120] Jae-Young Rho and George M Pharr. Effects of drying on the mechanical properties of bovine femur measured by nanoindentation. *Journal of Materials Science: Materials in Medicine*, 10(8):485–488, 1999.

[121] Jae-Young Rho, Ting Y Tsui, and George M Pharr. Elastic properties of human cortical and trabecular lamellar bone measured by nanoindentation. *Biomaterials*, 18(20):1325–1330, 1997.

[122] Ji Young Rho, Peter Zioupos, John D Currey, and George M Pharr. Microstructural elasticity and regional heterogeneity in human femoral bone of various ages examined by nano-indentation. *Journal of Biomechanics*, 35(2):189–198, 2002.

[123] Thomas Richard, Fabrice Dagrain, Edmond Poyol, and Emmanuel Detournay. Rock strength determination from scratch tests. *Engineering Geology*, 147:91–100, 2012.

[124] Thomas Richard, Emmanuel Detournay, Andrew Drescher, Pascal Nicodeme, Dominique Fourmaintraux, et al. The scratch test as a means to measure strength of sedimentary rocks. In *SPE/ISRM Rock Mechanics in Petroleum Engineering*. Society of Petroleum Engineers, 1998.

[125] RO Ritchie. Mechanisms of fatigue crack propagation in metals, ceramics and composites: role of crack tip shielding. *Materials Science and Engineering: A*, 103(1):15–28, 1988.

[126] Robert O Ritchie. How does human bone resist fracture? *Annals of the New York Academy of Sciences*, 1192(1):72–80, 2010.

[127] Robert O Ritchie, Markus J Buehler, and Paul Hansma. Plasticity and toughness in bone. *Phys Today*, 62(6):41–47, 2009.

[128] Robert O Ritchie, John H Kinney, Jamie J Kruzic, and Ravi K Nalla. A fracture mechanics and mechanistic approach to the failure of cortical bone. *Fatigue & Fracture of Engineering Materials & Structures*, 28(4):345–371, 2005.

[129] Diane Margel Robertson and Dennis C Smith. Compressive strength of mandibular bone as a function of microstructure and strain rate. *Journal of Biomechanics*, 11(10):455–471, 1978.

[130] Marcel E Roy, Jae-Young Rho, Ting Y Tsui, Neal D Evans, and George M Pharr. Mechanical and morphological variation of the human lumbar vertebral cortical and trabecular bone. *Journal of Biomedical Materials Research*, 44(2):191–197, 1999.

[131] Mitchell B Schaffler and David B Burr. Stiffness of compact bone: effects of porosity and density. *Journal of Biomechanics*, 21(1):13–16, 1988.

[132] G Schei, E Fjær, E Detournay, CJ Kenter, GF Fuh, F Zausa, et al. The scratch test: an attractive technique for determining strength and elastic properties of sedimentary rocks. In *SPE Annual Technical Conference and Exhibition*. Society of Petroleum Engineers, 2000.

[133] Ian N Sneddon. The relation between load and penetration in the axisymmetric boussinesq problem for a punch of arbitrary profile. *International Journal of Engineering Science*, 3(1):47–57, 1965.

[134] Ian Naismith Sneddon. Mixed boundary value problems in potential theory. 1966.

[135] Luca Sorelli, Georgios Constantinides, Franz-Josef Ulm, and François Toutlemonde. The nano-mechanical signature of ultra high performance concrete

by statistical nanoindentation techniques. *Cement and Concrete Research*, 38(12):1447–1456, 2008.

[136] NA Stilwell and D Tabor. Elastic recovery of conical indentations. *Proceedings of the Physical Society*, 78(2):169, 1961.

[137] David Tabor. *The hardness of metals*. Oxford University Press, 2000.

[138] Kuangshin Tai, Hang J Qi, and Christine Ortiz. Effect of mineral content on the nanoindentation properties and nanoscale deformation mechanisms of bovine tibial cortical bone. *Journal of Materials Science: Materials in Medicine*, 16(10):947–959, 2005.

[139] TY Tsui, WC Oliver, and GM Pharr. Influences of stress on the measurement of mechanical properties using nanoindentation: Part i. experimental studies in an aluminum alloy. *Journal of Materials Research*, 11(03):752–759, 1996.

[140] Charles H Turner, Jae Rho, Yuichi Takano, Ting Y Tsui, and George M Pharr. The elastic properties of trabecular and cortical bone tissues are similar: results from two microscopic measurement techniques. *Journal of Biomechanics*, 32(4):437–441, 1999.

[141] Franz-Josef Ulm, Matthieu Vandamme, Chris Bobko, Jose Alberto Ortega, Kuangshin Tai, and Christine Ortiz. Statistical indentation techniques for hydrated nanocomposites: concrete, bone, and shale. *Journal of the American Ceramic Society*, 90(9):2677–2692, 2007.

[142] Franz-Josef Ulm, Matthieu Vandamme, Hamlin M Jennings, James Vanzo, Michelle Bentivegna, Konrad J Krakowiak, Georgios Constantinides, Christopher P Bobko, and Krystyn J Van Vliet. Does microstructure matter for statis-

tical nanoindentation techniques? *Cement and Concrete Composites*, 32(1):92–99, 2010.

[143] WC Van Buskirk, SC Cowin, and Ro N Ward. Ultrasonic measurement of orthotropic elastic constants of bovine femoral bone. *Journal of Biomechanical Engineering*, 103(2):67–72, 1981.

[144] Matthieu Vandamme, Franz-Josef Ulm, and Philip Fonollosa. Nanogranular packing of c–s–h at substochiometric conditions. *Cement and Concrete Research*, 40(1):14–26, 2010.

[145] Mark R VanLandingham, John S Villarrubia, William F Guthrie, and Greg F Meyers. Nanoindentation of polymers: an overview. In *Macromolecular Symposia*, volume 167, pages 15–44. Wiley-Blackwell, 111 River Street Hoboken NJ 07030-5774 USA, 2001.

[146] D Vashishth, JC Behiri, and W Bonfield. Crack growth resistance in cortical bone: concept of microcrack toughening. *Journal of Biomechanics*, 30(8):763–769, 1997.

[147] D Vashishth, KE Tanner, and W Bonfield. Contribution, development and morphology of microcracking in cortical bone during crack propagation. *Journal of Biomechanics*, 33(9):1169–1174, 2000.

[148] Deepak Vashishth. Hierarchy of bone microdamage at multiple length scales. *International Journal of Fatigue*, 29(6):1024–1033, 2007.

[149] X Wang, YJ Yoon, and H Ji. A novel scratching approach for measuring age-related changes in the in situ toughness of bone. *Journal of Biomechanics*, 40(6):1401–1404, 2007.

[150] Xiaodu Wang and C Agrawal. Fracture toughness of bone using a compact sandwich specimen: Effects of sampling sites and crack orientations. *Journal of Biomedical Materials Research*, 33(1):13–21, 1996.

[151] Xiaodu Wang and C Agrawal. A mixed mode fracture toughness test of bone–biomaterial interfaces. *Journal of Biomedical Materials Research*, 53(6):664–672, 2000.

[152] Xiaodu Wang, Ruud A Bank, Johan M TeKoppele, and C Agrawal. The role of collagen in determining bone mechanical properties. *Journal of Orthopaedic Research*, 19(6):1021–1026, 2001.

[153] Xiaodu Wang, Jim Lankford, and C Agrawal. Use of a compact sandwich specimen to evaluate fracture toughness and interfacial bonding of bone. *Journal of Applied Biomaterials*, 5(4):315–323, 1994.

[154] Ulrike GK Wegst, Hao Bai, Eduardo Saiz, Antoni P Tomsia, and Robert O Ritchie. Bioinspired structural materials. *Nature Materials*, 14(1):23–36, 2015.

[155] Steve Weiner and H Daniel Wagner. The material bone: structure-mechanical function relations. *Annual Review of Materials Science*, 28(1):271–298, 1998.

[156] TE Wenzel, MB Schaffler, and David P Fyhrie. In vivo trabecular microcracks in human vertebral bone. *Bone*, 19(2):89–95, 1996.

[157] TM Wright and WC Hayes. Fracture mechanics parameters for compact bone—effects of density and specimen thickness. *Journal of Biomechanics*, 10(7):419–430, 1977.

[158] Jiahau Yan, Kari B Clifton, John J Mecholsky, and Roger L Reep. Fracture toughness of manatee rib and bovine femur using a chevron-notched beam test. *Journal of Biomechanics*, 39(6):1066–1074, 2006.

[159] Jiahau Yan, John J Mecholsky, and Kari B Clifton. How tough is bone? application of elastic–plastic fracture mechanics to bone. *Bone*, 40(2):479–484, 2007.

[160] Yener N Yeni and David P Fyhrie. A rate-dependent microcrack-bridging model that can explain the strain rate dependency of cortical bone apparent yield strength. *Journal of Biomechanics*, 36(9):1343–1353, 2003.

[161] Liang-Chi Zhang and Hiroaki Tanaka. On the mechanics and physics in the nano-indentation of silicon monocrystals. *JSME International Journal Series A Solid Mechanics and Material Engineering*, 42(4):546–559, 1999.

[162] Elizabeth A Zimmermann, Holly D Barth, and Robert O Ritchie. The multiscale origins of fracture resistance in human bone and its biological degradation. *Jom*, 64(4):486–493, 2012.

[163] Elizabeth A Zimmermann, Bernd Gludovatz, Eric Schaible, Björn Busse, and Robert O Ritchie. Fracture resistance of human cortical bone across multiple length-scales at physiological strain rates. *Biomaterials*, 35(21):5472–5481, 2014.

[164] Elizabeth A Zimmermann, Eric Schaible, Hrishikesh Bale, Holly D Barth, Simon Y Tang, Peter Reichert, Bjoern Busse, Tamara Alliston, Joel W Ager, and Robert O Ritchie. Age-related changes in the plasticity and toughness of human cortical bone at multiple length scales. *Proceedings of the National Academy of Sciences*, 108(35):14416–14421, 2011.

[165] P Zioupos and JD Currey. Changes in the stiffness, strength, and toughness of human cortical bone with age. *Bone*, 22(1):57–66, 1998.

[166] Philippe K Zysset, X Edward Guo, C Edward Hoffler, Kristin E Moore, and Steven A Goldstein. Elastic modulus and hardness of cortical and trabecular bone lamellae measured by nanoindentation in the human femur. *Journal of Biomechanics*, 32(10):1005–1012, 1999.

[167] PK Zysset. Indentation of bone tissue: a short review. *Osteoporosis International*, 20(6):1049–1055, 2009.